communications biology

A Nature Portfolio journal

Article

https://doi.org/10.1038/s42003-025-07883-6

A bovine pulmosphere model and multiomics reveal early host response signature in tuberculosis

Vinay Bhaskar[1], Rishi Kumar[1,2], Manas Ranjan Praharaj[1,2], Sripratyusha Gandham[1,2], Hemanta Kumar Maity[3], Uttam Sarkar[4] & Bappaditya Dey[1,2]

Early interactions between tubercle bacilli and lung cells are critical in tuberculosis (TB) pathogenesis. Conventional two-dimensional cell cultures fail to replicate the multicellular complexity of lungs. We introduce a three-dimensional pulmosphere model for *Mycobacterium tuberculosis* infection in bovine systems, demonstrating through comprehensive transcriptome and proteome analyses that these multicellular spheroids closely mimic lung cell diversity, interactions, and extracellular matrix (ECM) composition. Cell viability, hypoxia, and reactive oxygen species assessments over three weeks confirm the model's suitability. To establish infection, we employed *M. bovis* BCG—an attenuated vaccine strain, and *M. tuberculosis* H37Rv—a laboratory adapted human clinical strain that is attenuated for cattle infection compared to *M. bovis*. Both infection upregulated key host pathways; however, *M. tuberculosis* induced distinct responses, including enhanced ECM receptors expression, neutrophil chemotaxis, interferon signaling, and RIG-1 signaling. A six genes/protein signature- IRF1, CCL5, CXCL8, CXCL10, SERPINE1, and CFB -emerges as an early host response marker to *M. tuberculosis* infection. Infection with virulent *M. bovis* and *M. orygis* revealed a shared upregulated gene signature across Mycobacterium tuberculosis complex species, but with pathogen-specific variations. This study presents a robust ex vivo bovine pulmosphere TB model with implications in biomarkers discovery, high-throughput drug screening, and TB control strategies.

Tuberculosis (TB) in bovines poses a substantial challenge to global livestock economy and public health. *Mycobacterium bovis* and *M. tuberculosis* are the leading members of the Mycobacterium tuberculosis complex (MTBC) causing bovine TB (BTB)[1,2]. The recent addition of *M. orygis* to this group further emphasizes the critical risk of zoonotic transmission to humans[3]. The presence of drug-resistant tubercle bacteria in both humans and cattle complicates TB eradication efforts, as cattle may act as reservoirs for drug-resistant strains[4]. This underscores the need to address bovine TB as a pressing global public health priority.

In many Southeast Asian countries, such as India, where BTB incidence rates range from 2 to 50%, combating BTB is hindered by its complex epidemiology, challenges in implementing effective eradication policies, and the absence of suitable diagnostics and vaccines[5,6]. Additionally, the lack of species-specific disease models, and limited research infrastructure such as large animal biosafety level 3 facilities, further constrain research efforts to study BTB pathobiology and devising its control strategies. Current understanding of immune responses in BTB primarily relies on in vitro bovine PBMCs infection models, and a limited range of cattle in vivo infection studies[7–9]. Additionally, bovine primary alveolar macrophages, mouse and human macrophage cell lines have also been utilized to model host–pathogen interaction during early stages of BTB[10–13]. However, the variation in immune responses among different host species, and different organs underscores the importance of developing bovine lung-based models to unravel the intricacies of bovine pulmonary TB[14,15]. In vitro disease models that replicate lung cellular environments and granulomatous TB pathology are crucial, particularly in settings with limited bio-containment resources, to broaden the scope of research on BTB pathogenesis.

In recent years, three-dimensional (3D) lung cell culture systems have gained traction in studying TB and respiratory diseases due to their advantages over conventional two-dimensional (2D) cell culture methods[16–18]. While some 3D lung culture systems allow for the formation of cellular structures that resemble the lung tissue, including the presence of

[1]National Institute of Animal Biotechnology, Hyderabad, Telangana, India. [2]Regional Centre for Biotechnology, Faridabad, Haryana, India. [3]Department of Avian Sciences, West Bengal University of Animal and Fishery Sciences, Kolkata, West Bengal, India. [4]Department of Animal Genetics and Breeding, West Bengal University of Animal and Fishery Sciences, Kolkata, West Bengal, India. e-mail: bdey@niab.org.in

alveoli and airway epithelium, others offer improved multi-cellular cell–cell and cell–matrix interactions, allowing for enhanced cell differentiation, migration, and signaling[19–21]. These advancements enable researchers to investigate the interactions between lung cells and pathogens, environmental stimuli, and therapeutic compounds, leading to more accurate predictions and translation to pulmonary disease biology[22].

In this study, we developed a multicellular 3D pulmosphere model using bovine primary lung cells to advance our understanding of BTB pathogenesis and host responses during early stage of infection. By mimicking the multicellularity, greater cell-cell, and cell-matrix interactions, this model offers a unique platform to study the intricate interactions between the tubercle bacilli and lung cells of the bovine host. Comprehensive transcriptomic and proteomic analyses following infection with *M. bovis* BCG and *M. tuberculosis* H37Rv—a virulent human tubercle bacillus attenuated in bovine infection—revealed key signaling and metabolic pathways, along with differentially expressed genes and proteins involved in early infection[23,24]. These findings were further validated through qPCR-based gene expression analysis following infection with virulent *M. bovis* and *M. orygis*. This paves the way for discovering BTB disease biomarkers, correlates of TB immunity, and potential targets for host-directed therapies. In addition to providing a new bovine 3D pulmosphere TB model, this study enhances our understanding of TB pathogenesis, potentially informing efforts aimed at developing effective prevention and control strategies.

Results

Development of bovine primary lung cell-derived pulmosphere

To establish a pulmosphere model for the study of ex vivo TB infection, first, the method for generation of pulmospheres from bovine primary lung mixed cells population was optimized. Figure 1A depicts the overall workflow used for the generation of the pulmosphere. To optimize the formation of uniform spheroids, four different seeding densities of the mixed primary lung cells per well were evaluated, including 1×10^4, 1.5×10^4, 2×10^4, and 2.5×10^4 cells in a U bottom 96-well tissue culture plate. Notably, round-shaped, self-assembled, and reproducible spheroids were generated within 24 h following centrifugation-based spheroid assembly (Fig. 1B). The optimum seeding densities were found to be 1×10^4 and 1.5×10^4 cells per well, while a higher number of cells resulted in an improper assembly leading to irregularly shaped cell clumps. Figure 1C depicts the relative number of spheroids generated at different cell seeding concentrations. These findings indicated that Poly-HEMA-coated U-bottom plates provided an appropriate surface for pulmosphere development at the calibrated cell densities. Over a monitoring period of 28 days, the growth dynamics of bovine lung multi-cell spheroids were characterized. The mean diameter of the spheroids increased from 494 ± 70.58 µm at Day 7 post-sphere formation to 1205.4 ± 106.76 µm at Day 28 ($n = 20$), revealing a substantial expansion in size over 4 weeks (Fig. 1D, E). Further, the influence of primary lung cell culture passage number on pulmosphere formation was explored. Cells from passages zero and one lead to proper spheroid formation, while cells from the latter passages reduced the success rate of spheroid formation as well as resulted in irregular-shaped cell clumps (Supplementary Fig. 1A, B). This relationship suggests a significant impact of the passage number on spheroid morphology and integrity, underscoring the importance of early passages for maintaining the characteristics of pulmospheres derived from primary lung cells.

Assessment of live and dead cells in pulmospheres

To further extend the characterization of pulmospheres, we conducted a live-dead cell assessment for a period of 21 days to monitor changes in cell viability and the progression of cell death within the pulmospheres over

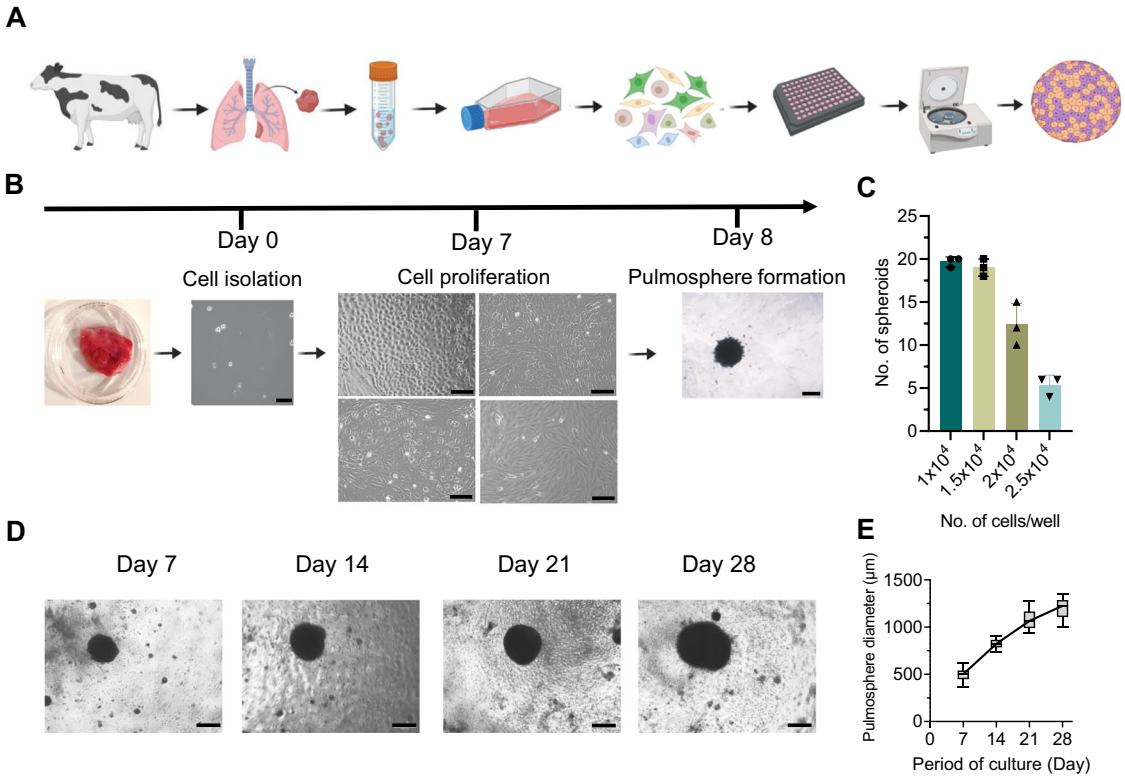

Fig. 1 | Generation and morphological characterization of bovine 3D pulmosphere. A Schematic cartoon representation of the protocol for bovine 3D pulmosphere development. Illustration was made using Biorender. **B** Bovine lung primary cells were isolated and grown for 7 days showing multiple cell types, pulmosphere was assembled and images were taken after 24 h. Scale bars: 400 µm for 4× images (Day 0, day 7) and 200 µm for 10× images (Day 8). **C** Bar graph depicts the average number of compact pulmospheres formed with respect to the different cell seeding densities. Individual data points represent biological replicates ($n = 3$). **D** Representative images of pulmospheres captured at every week till 28 days. **E** The box plot depicts the relative size of pulmospheres over the period of culture ($n = 20$). Scale bars: 400 µm for 4× images. Data information: In (**C**, **E**) data are presented as mean ± sd. Statistical analysis included an unpaired two-tailed t-test for comparison between two. A 95% confidence interval or 0.05 threshold for significance ($p < 0.05$) was used in statistical tests.

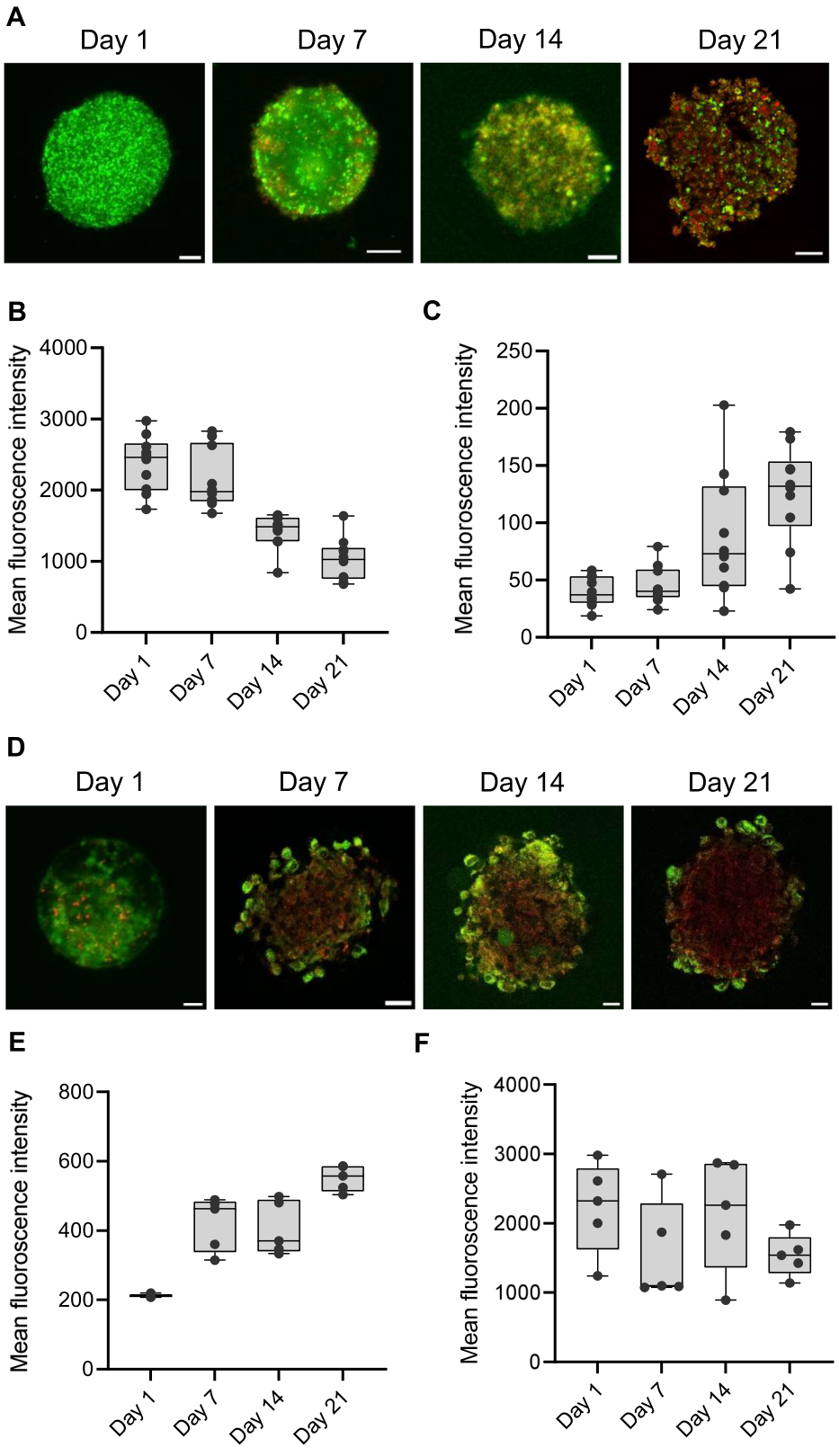

Fig. 2 | Assessment of live/dead, hypoxia, and ROS in pulmospheres. A Representative images of live/dead cells in pulmospheres at Day 1, 7, 14, and 21. Live cells are stained with CFSC (Green) and dead cells are stained with PI (Red). The box plot represents the mean fluorescence intensity of (**B**) CFSE-stained live cell green fluorescence and (**C**) dead cell red fluorescence of the pulmospheres ($n = 10$) over 21 days experimental period. **D** The representative images of Hypoxia (Red) and ROS (Green) status in the pulmospheres. The box plot represents the mean fluorescence intensity of Hypoxia (**E**) and ROS (**F**) levels over the experimental period ($n = 5$). Images were captured using a Super-Resolution Microscope in Airyscan mode. Fluorescence values were measured using a wide-field fluorescence microscope. The scale bar represents 20 µm, 40× magnification.

time. For this, cells were stained with carboxyfluorescein succinimidyl ester (CFSE) and propidium iodide (PI), where CFSE selectively labels live and actively proliferating cells, and PI specifically stains non-viable cells (Fig. 2A). The box plot represents the mean fluorescence intensity of CFSE-stained live cells (Fig. 2B) and PI-stained dead cells (Fig. 2C), providing a quantitative measure of both live and dead cells at each time point within the pulmosphere. The results reveal a clear trend of increasing number of dead cells as the incubation period progresses, which is in contrast to the reducing number of live cells. From Day 1 till Day 7, the CFSE fluorescence was more less stable with minimal PI fluorescence, indicating a negligible dead cell population within the pulmospheres during the early phase of pulmosphere growth (Supplementary movies 1, 2), A sharp slope of the PI fluorescence from Day 7 to Day 14 indicate a rise in dead cell population, which increases considerably by Day 21 (Supplementary movie 3, 4). This pronounced

increase in dead cell population highlights a cumulative effect of environmental stressors such as nutrient depletion, hypoxia, and oxidative stress within the 3D structure towards the later stage of pulmosphere growth.

Hypoxia and oxidative stress conditions in 3D pulmospheres

Spheroid or organoid cultures often develop oxygen gradients due to limited diffusion of oxygen and nutrients to the inner core leading to heterogeneous cell populations, including hypoxic cores, proliferative zones, and necrotic regions[25]. Hypoxia and reactive oxygen species (ROS) levels play critical roles not only in determining the physiological status of model system but also influences effectiveness of the intended therapy. Hence, next, we evaluated hypoxia and oxidative stress status in the pulmospheres using the ROS-ID® Hypoxia/Oxidative Stress Detection Kit (Enzo Life Sciences, Inc.). Figure 2D shows a representative image of the central z-stack of pulmospheres, providing a focused view of the hypoxia and ROS distribution within a specific depth. However, the distribution of ROS and hypoxia signals varies across different z-stacks due to the heterogeneous nature of the 3D structure of the pulmospheres (Supplementary movies 5, 6, 7, 8). The box plot reflects the mean fluorescence intensity derived from the maximum intensity projections across all z-stacks, offering a comprehensive and averaged representation of the overall hypoxia (Fig. 2E) and ROS levels within the pulmospheres (Fig. 2F). The fluorescence intensity depicting hypoxia levels show a significant increase from Day 1 to Day 7, which remained steady till Day 14, and subsequently exhibited sharp increase by Day 21. This indicates that as the pulmospheres mature, the core regions become increasingly oxygen-deprived due to potentially limited diffusion of oxygen. Unlike hypoxia, ROS levels in the pulmospheres were found to exhibit a distinct bimodal curve with a drop in ROS levels at Day 7 compared to the levels at Day 1, surging back to initial levels by Day 14, and again dropping considerably by Day21 (Supplementary movies 5,6,7,8). While hypoxia consistently increases over time, ROS levels do not follow the same linear pattern highlighting the complexity of cellular responses in 3D environment.

3D pulmospheres recapitulate cellular heterogeneity and extracellular matrix enrichment over 2D monolayer culture

To investigate the multicellularity of the 3D pulmospheres and their functional profile we performed liquid chromatography-mass spectrometry (LC-MS) analysis of the whole protein extract 24 h post-assembly of the pulmospheres. The proteomics workflow is provided in Supplementary Fig 2. A pool of 2748 peptides was detected in the proteome of the pulmospheres (Supplementary data 1), which were then subjected to global cell-type-specific enrichment analysis using the web-based tool WebCSEA[26], that unveiled the presence of 17 cell types (Fig. 3A). Further analysis of lung tissue-specific cell typing reveals 32 different types of lung cells encompassing epithelial, endothelial, fibroblast, pneumocytes, and an array of immune cells including macrophage, dendritic cells, neutrophil, T-cell, B-cells, plasma cells, etc. highlighting the complex multi-cellularity of the pulmosphere (Fig. 3B). A comparative assessment of protein expression patterns was performed between 2D monolayer cells, and 3D pulmospheres at 24 h post-culture to understand the functional differences between two culture systems. Supplementary Fig 3 A-C, depicts the comparative omics analysis features: (A) Volcano plot, (B) PCA analysis, and (C) hierarchical clustering of peptide abundance) of the DEPs of 3D vs. 2D culture proteome.

Strikingly, upon gene-ontology analysis (GO) of cellular components, a pronounced upregulation of the fibrinogen complex and collagen-containing extracellular matrix (ECM) proteins were found in the case of 3D pulmospheres (Fig. 3C). Subsequent analysis of these proteins using a matrisome database revealed a strong association of the majority of the core matrisome and matrisome-associated proteins in the case of 3D pulmospheres[27] (Fig. 3D). This finding suggests a fundamental shift in the protein expression profile in the 3D spheroids that emphasizes the significance of the 3D cellular organization compared to 2D in promoting the deposition of ECM components, which are integral part of lung basement membrane. Further insight into the upregulated ECM network within the 3D pulmosphere was gained through the identification of closely interconnected ECM proteins by STRING analysis (Fig. 3E). The top 15 major ECM proteins showing a higher number of interconnected nodes were APOH, APOA1, HPX, AMBP, APCS, APOE, AHSG, A2M, SERPINC1, PLG, FGG, F2, FGA, FGB, KNG1 (Fig. 3F). In the context of lung ECM formation, FGA, FGB, and FGG contribute to the ECM assembly through fibrin formation and provide structural integrity of the ECM. A2M and KNG1 are associated with protease inhibition, potentially regulating ECM remodeling processes. APOA1, APOE, and HPX are involved in lipid metabolism and transport, which can influence ECM stability. AMBP, APCS, APOH, and AHSG contribute to ECM formation by interacting with ECM proteins and also contribute modulation of inflammation and cell adhesion response. This intricate web of ECM components highlights the dynamic interactions and organization that contribute to the pulmosphere integrity and functionality. In addition to the upregulation of ECM proteins, several biological pathways were upregulated in the pulmosphere (Supplementary data 2). These include tissue homeostasis, epithelial cell proliferation, positive regulation of cell development, regulation of vasculature development, response to wounding, humoral immune response, negative regulation of apoptotic signaling pathway, and response to oxidative stress, etc. indicate that our 3D model not only captures the diverse cell types present in the lungs but also represents the complex extracellular matrix milieu pivotal for integrity of multicellular spheroid. To validate the reproducibility and consistency of the cellular composition in the pulmospheres and the ECM components, subsequently we analyzed the statistical variation of these parameters in the transcriptome data across 3 biological replicates, and no significant variability was observed between the pulmospheres (Supplementary Fig. 4A, B). The collective presence of distinct cell populations and ECM proteins underscores the relevance of the 3D model in recapitulating the complexity of the lung microenvironment.

Development of pulmosphere TB disease model

The establishment of a bovine pulmosphere TB disease model represents an advancement, offering a platform for thorough exploration into the complex interplays between *M. tuberculosis* or *M. bovis* and bovine lung cells within a relevant context. To construct the bovine TB infection model, both virulent *M. tuberculosis* and the vaccine strain *M. bovis* Bacille Calmette-Guérin (BCG) were employed. The inclusion of the vaccine strain enabled a comparative analysis of the host response elicited by a virulent *M. tuberculosis* strain versus an avirulent *M. bovis* BCG strain. For real-time monitoring of infection dynamics, fluorescent protein-expressing variants of *M. tuberculosis* and *M. bovis* BCG were used[28]. Figure 4A depicts the workflow employed for the generation of the pulmosphere TB infection model. Seven days following the culture of bovine primary lung cells, the cells were subjected to infection with a pre-calibrated multiplicity of infection (MOI) of 1:10. This time point was chosen to harness the maximal heterogeneity of cell types inherent to early-passage of primary lung cells, ensuring an optimal representation of the multicellular microenvironment in the development of the disease models. After infection, lung cells were assembled into 3D pulmospheres using the same methodology established for the formation of uninfected 3D pulmospheres. The infected 3D pulmospheres were monitored over 21 days through live fluorescence microscopy at weekly intervals (Fig. 4B). This longitudinal observation unveiled distinctive infection patterns between the attenuated vaccine strain *M. bovis* BCG and the virulent *M. tuberculosis* strain. The BCG strain exhibited restrained replication within the pulmospheres throughout the three-week study, predominantly localizing to focal infection. In stark contrast, the virulent *M. tuberculosis* strain demonstrated unhindered replication throughout infection and displayed widespread dissemination to all regions of the pulmospheres from the initial foci of infection (Fig. 4B). The successful establishment of the bovine 3D pulmosphere TB infection model has ushered in the ability to visualize the progression of infection dynamics ex vivo. This dynamic system provides a unique window into the complex interplay between mycobacterium species and bovine lung cells, facilitating further studies to understand the deeper insights into the mechanisms underpinning TB pathogenesis.

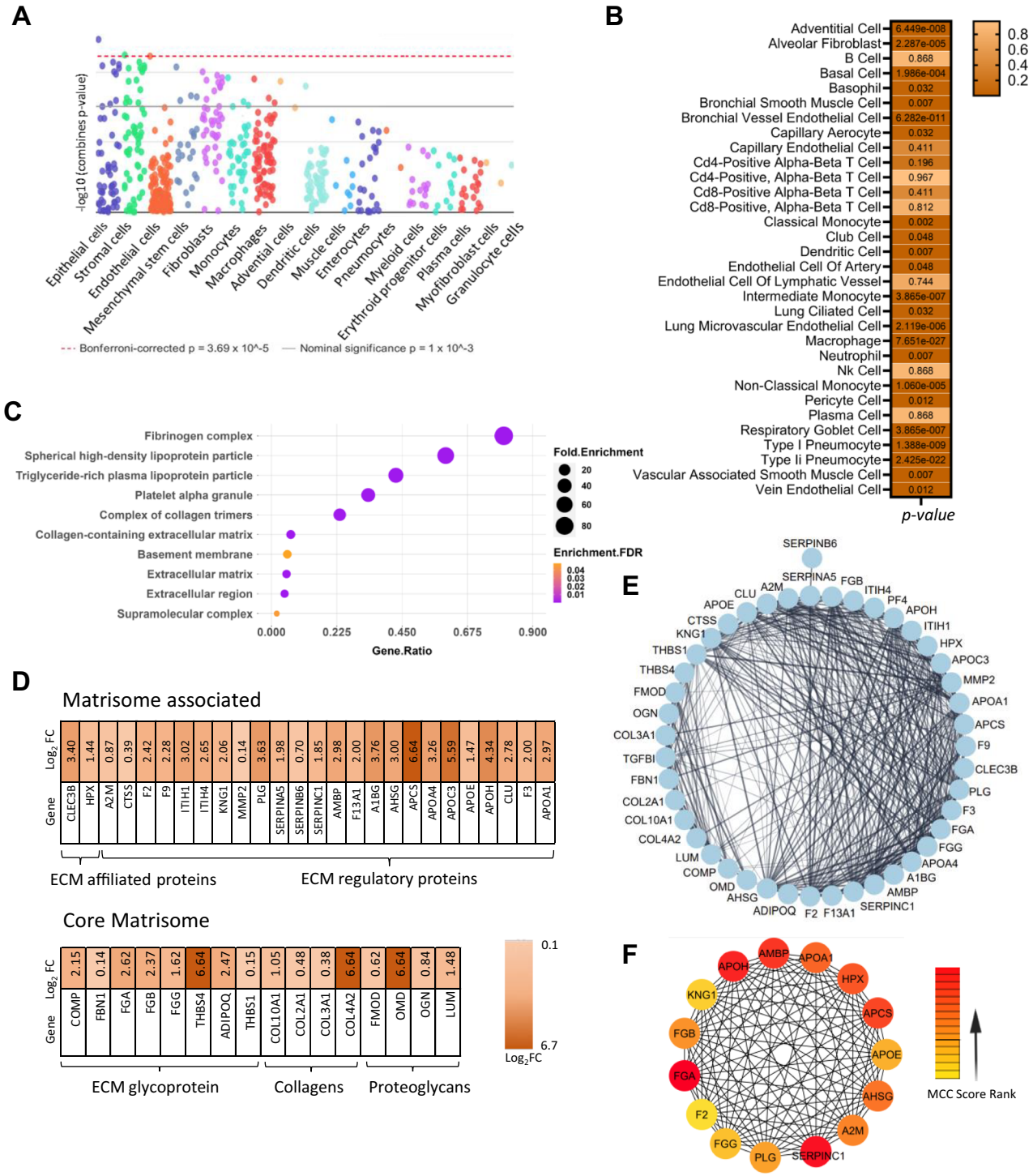

Fig. 3 | Cellular composition of 3D pulmosphere and key upregulated PPI networks over 2D culture. A Array of different cell types identified in bovine 3D Pulmosphere using WebCSEA. **B** Lung-tissue specific cell type enrichment analysis using "Tabula Sapiens" single cell analysis showed the presence of 22 cell types as significantly enriched, $p < 0.05$. **C** Gene Ontology of cellular composition in 3D pulmosphere vs monolayer 2D lung cell culture. **D** Protein expression profile of ECM and associated proteins in 3D pulmosphere. **E** Densely interconnected protein network of ECM proteins derived via STRING analysis. **F** Top 15 critical hub genes involved in the structural organization of 3D pulmosphere were identified using Cyto-Hubba, a Cytoscape plug-in.

Transcriptomic and proteomic analysis of host response to BCG and *M. tuberculosis* infection in pulmosphere model

To decipher the intricate host–pathogen interactions occurring at the early phase of infection, we analyzed the global transcriptomic and proteomic patterns of the infected and uninfected pulmospheres at 24 h post-sphere formation. A stringent analytical framework was employed, wherein genes and proteins demonstrating at least a 2-fold change, and with an adjusted p-value of <0.05 were deemed differentially expressed. The proteome and transcriptome data analysis workflow were provided in Supplementary Figs. 2 and 5, respectively. Supplementary Figs. 6A-D and 7A-E depict the comparative omics analysis features (Volcano plot, PCA analysis, and hierarchical clustering) of the transcriptome data for PS-BCG and PS-*M. tb* compared to uninfected pulmospheres, respectively. Comparative analysis revealed that the bovine pulmospheres exhibited substantial transcriptional

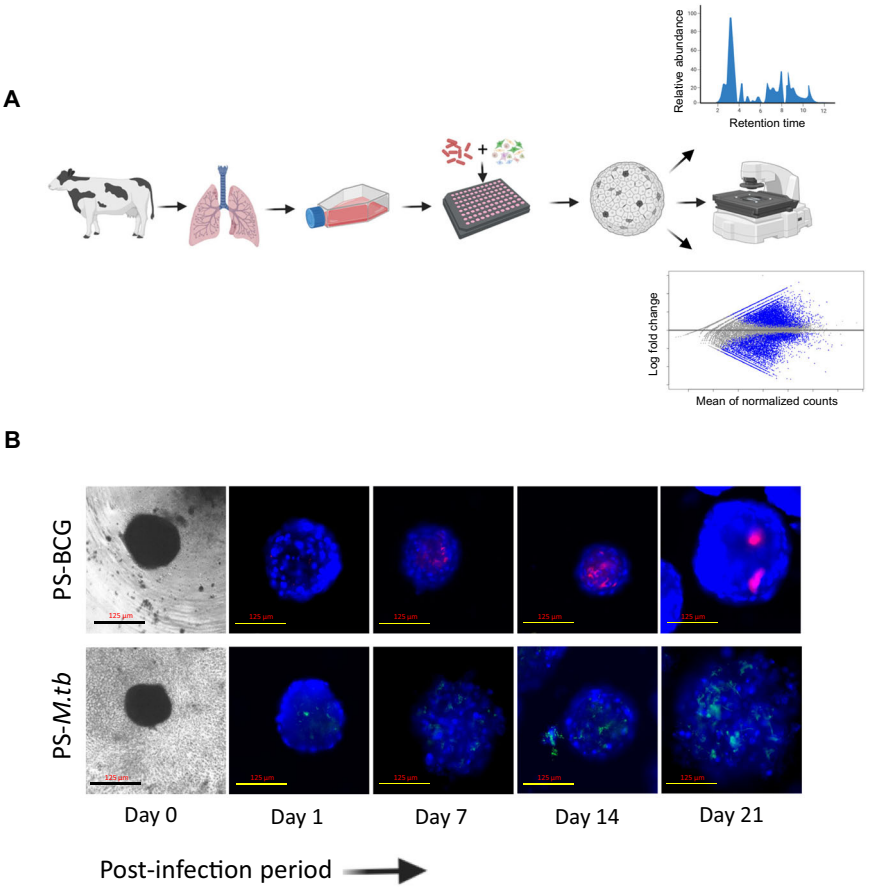

Fig. 4 | Establishment of bovine 3D pulmosphere TB infection model. A Schematic cartoon representation of the protocol for the establishment of bovine 3D pulmosphere infection and downstream analysis. Illustration was made using Biorender. **B** Seven-day cultures of bovine primary lung cells were infected with either *M. bovis* BCG-mCherry or *M. tb*-eGFP at an MOI of 1:10 and pulmospheres were assembled (Day 0), and monitored under live cell imaging fluorescence microscope weekly till 21 days. The figures depict representative photographs of infected pulmospheres at different time points. The scale bars represent 125 µm for 10× images.

and proteomic responses upon infection with *M. bovis* BCG and *M. tuberculosis* strains (Figs. 5, 6). Specifically, 766 differentially expressed genes, and 281 differentially expressed proteins were identified in *M. bovis* BCG-infected pulmospheres, whereas 2129 DEGs and 402 DEPs were detected in *M. tuberculosis*-infected pulmospheres, relative to uninfected counterparts indicating that a greater number of genes exhibited altered expression levels in response to the virulent *M. tuberculosis* challenge, both at the transcript and protein levels (Fig. 5A, B). Further, compared to BCG infection 3828 genes and 406 proteins were differentially expressed in the case *of M. tuberculosis* infection (Fig. 5A, B). This finding underlines the intricate and multifaceted nature of the host response to *M. tuberculosis* infection when compared with the avirulent *M. bovis* BCG-induced response. Additionally, a comparison with the publicly available transcriptome data from a variety of *M. tuberculosis* infection models employed by several previous studies revealed that the number of DEGs in our pulmosphere model was notably higher following *M. tuberculosis* infection (Fig. 5C)[7,10,29–32]. This finding highlights the 3D pulmosphere as a more robust system compared to the single-cell, or PBMC-based models representing an enormous depth of complexity and cellular responses induced during *M. tuberculosis* infection.

Functional enrichment analysis of differentially expressed genes following *M. tuberculosis* and *M. bovis* BCG infection

To gain insights into the biological implications of the observed differential expression, we performed GO and Kyoto Encyclopaedia of Genes and Genomes (KEGG) pathway enrichment analyses on upregulated and downregulated genes and proteins. Functional enrichment of the upregulated DEGs into the biological process via GO analysis reveals three major themes within the top-25 GO terms: immune response, cellular organization and ECM modification, and lipid metabolism were up-regulated in BCG-infected pulmosphere compared with the uninfected pulmosphere (Fig. 5D). Pathways related to activation of innate immune responses, *IFN-γ, TNF-α, IL-1β, IL-6* production, leukocyte aggregation, and acute phase response were upregulated in the case of BCG infection. In contrast, clusters of genes belonging to leukocyte activation, differentiation, proliferation, and chemotaxis were downregulated (Supplementary Fig. 8A). Further, KEGG pathway analysis of the DEGs in the BCG group showed additional upregulation of IL-17, TGF-beta, Cytosolic DNA sensing pathway, PPAR, and NF-kappa B signaling pathways as major immune-related pathways (Fig. 5E). In contrast, the top-down regulated immune pathways were complemented and coagulation cascades, neutrophil extracellular trap formation, Rap 1 signaling pathway, and Toll-like receptor signaling pathway (Supplementary Fig. 8 B).

Functional enrichment via GO analysis of the DEPs in the BCG-infected pulmospheres reveals significant upregulation of similar immune response-related genes and lipid biosynthetic pathways as observed in the case of DEGs, however, several additional metabolic pathways such as carboxylic acid biosynthesis, amide metabolism, and mRNA metabolic processes, etc. were found to be upregulated (Fig. 5F). However, KEGG pathway analysis did not show any significantly upregulated pathway (Fig. 5G). GO analysis of the downregulated proteins showed oxidative phosphorylation, AGE-RAGE signaling, Th17 differentiation, and NOD-like receptor signaling pathway as the major enriched pathways (Supplementary Fig. 9A). KEGG analysis of DEPs identified downregulation of pathways related to several cancer types, phagocytosis, adipocytokine signaling, and RIG-I-like receptor signaling (Supplementary Fig. 9 B).

On the other hand, in the case of *M. tuberculosis* infection, the immune response related to GO-BP terms shows upregulation of Th-17, Th-2 (IL-4), acute phase response, and genes related to negative regulation of IL-1, IL-2 production, and apoptotic signaling pathway (Fig. 6A). Additionally, the KEGG pathway analysis indicated AGE-RAGE signaling pathway, RIG-1-like receptor signaling pathways, ECM-Receptor interaction, mitophagy, TNF and IL-17 signaling pathways, MAPK Signaling, RAP-1, and HIF-1 signaling pathways as some of the leading upregulated pathways in case of

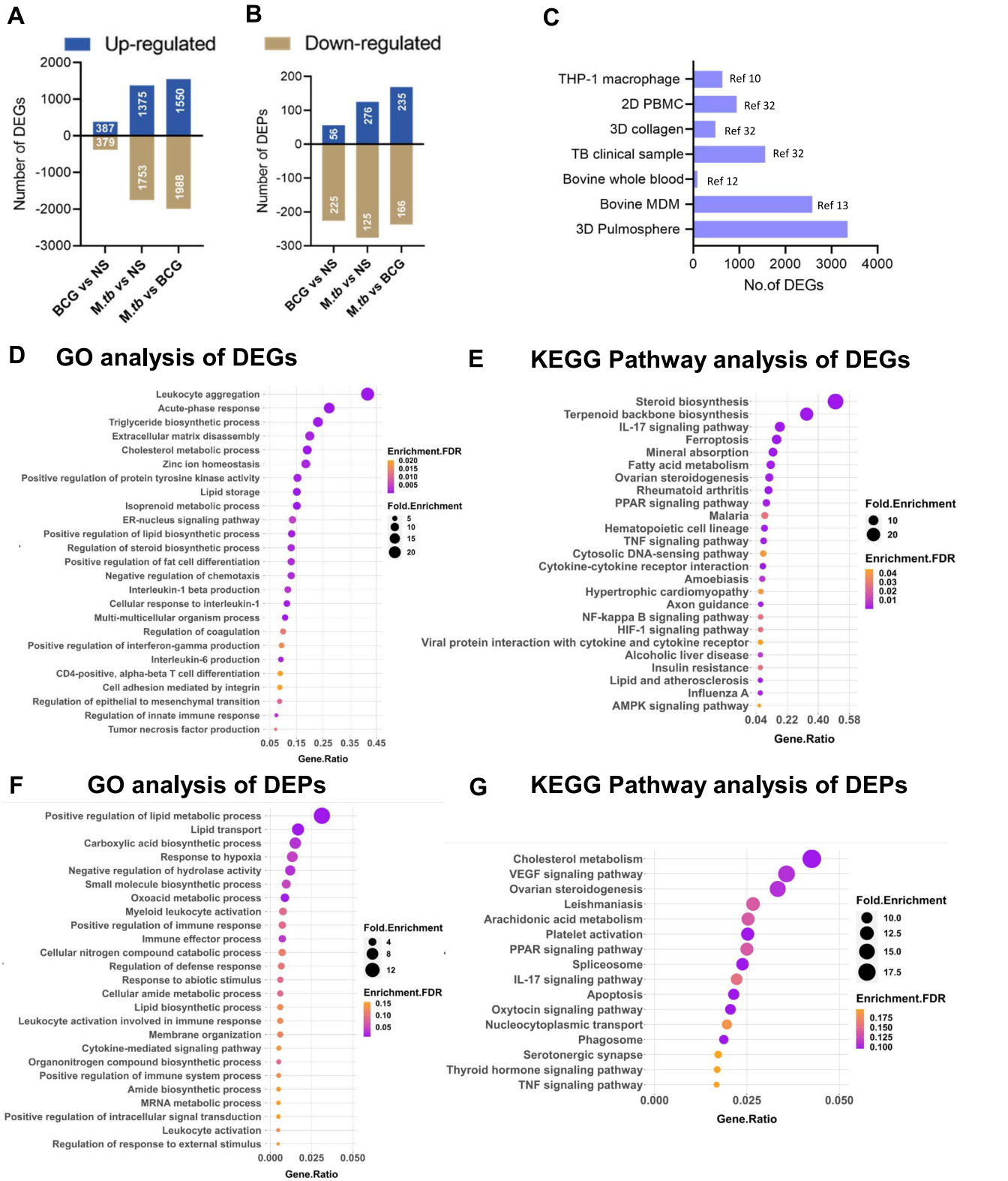

Fig. 5 | Differential gene, protein expression, and functional enrichment analysis of the DEGs and DEPs in 3D pulmospheres following BCG and *M. tuberculosis* infection. A No. of differentially expressed proteins in BCG and *M. tb* infected pulmospheres. **B** No. of differentially expressed genes in BCG and *M. tb* infected pulmospheres. **C** Comparative view of the DEG no. in PS-*M. tb* (this study) and selected TB infection model reported previously. The numbers in the parenthesis are the corresponding references. Biological processes (**D**), and KEGG pathway analysis of DEGs (**E**) of PS-BCG over uninfected pulmospheres. FDR < 0.05, and gene number >5 in a pathway were used as cutoff values. Biological processes (**F**), and KEGG pathway analysis of DEPs (**G**) of PS-BCG over uninfected pulmospheres, respectively. FDR < 0.05, and gene number >5 in a pathway were used as cutoff values.

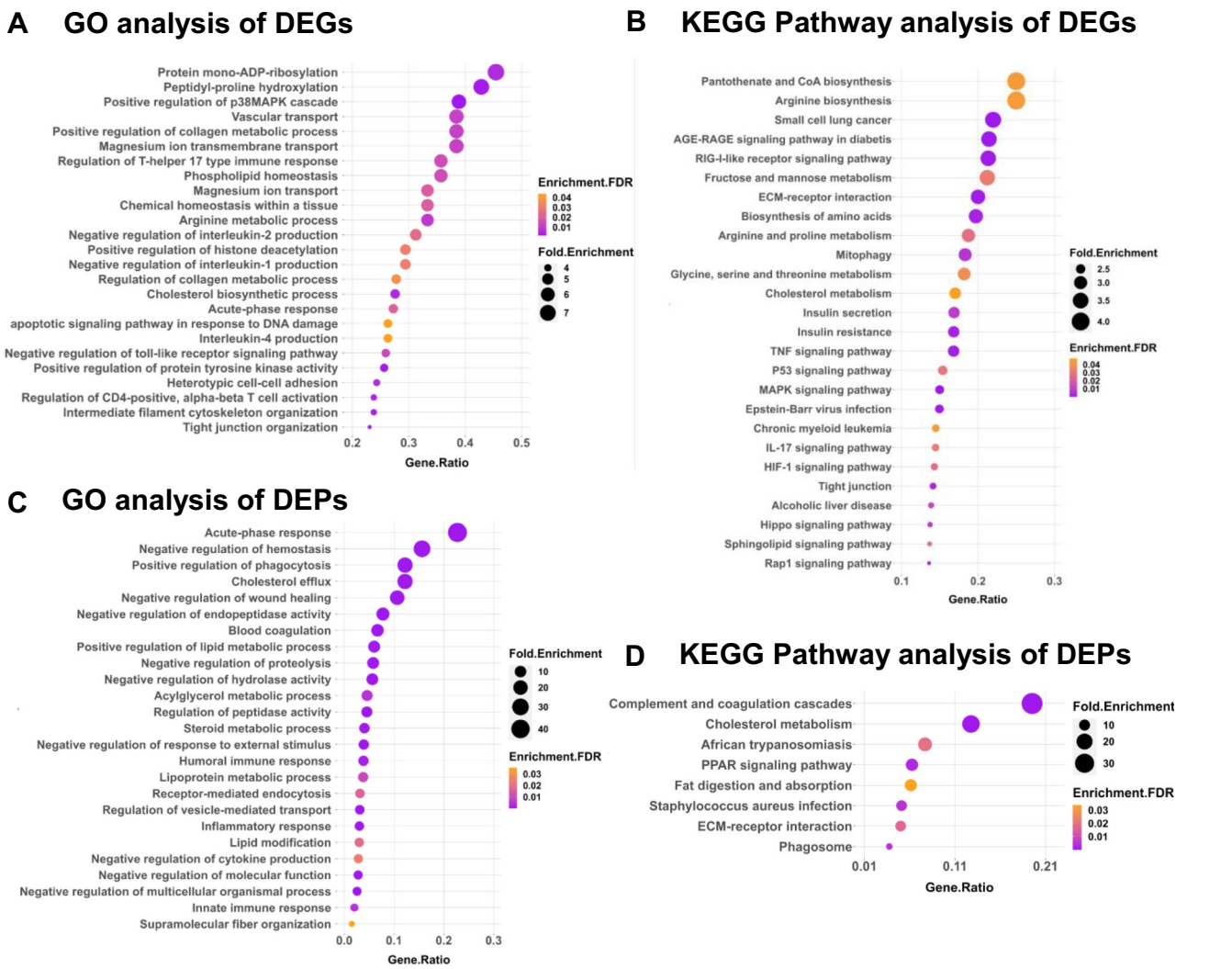

Fig. 6 | Functional enrichment analysis of the up-regulated genes and proteins in case of *M. tuberculosis* infection vs. uninfected pulmospheres. Biological processes (**A**) and KEGG pathway (**B**) analysis of DEGs of PS-*M.tb* over uninfected pulmospheres FDR < 0.05, and gene number >5 in a pathway were used as cutoff values. **C**, **D** Biological processes (**A**) and KEGG pathway (**B**) analysis of DEPs of PS-*M.tb* over uninfected pulmospheres FDR < 0.05, and gene number >5 in a pathway were used as cutoff values.

M. tuberculosis-infected pulmosphere (Fig. 6B). Whereas, the down-regulated pathways include complement and coagulation cascades, cell cycle process, ribosome biogenesis pathways, and neutrophil extracellular trap formation pathways (Supplementary Fig. 10A). KEGG analysis identifies mitochondrial respiratory chain complex assembly as one of the major downregulated pathways (Supplementary Fig. 10 B).

Functional enrichment via GO analysis of the DEPs in the case of *M. tuberculosis* infection led to the upregulation of several biological processes under GO-BP terms including acute phase response, Cholesterol, and lipid metabolism, positive regulation of phagocytosis, negative regulation of wound healing, humoral immune response, inflammatory and innate immune response (Fig. 6C), However, KEGG pathway analysis reveals upregulation of additional pathways, such as the complement and coagulation cascades, PPAR signaling pathway, and ECM- Receptor interaction in case of *M. tuberculosis* infection (Fig. 6D), Notably, both GO-BP terms and the KEGG pathways involving the downregulated genes remain similar to that of the DEGs, respectively (Supplementary Fig. 11A, B).

Protein interaction network, hub genes, and functional clusters

Next, to have an in-depth understanding of the functional interactions among DEGs, we constructed protein-protein interactions (PPI) maps using STRING software, and identified the potential interacting network of proteins (Supplementary data 3). The significantly interacting proteins from STRING analysis were subsequently analyzed via the molecular complex detection (MCODE) algorithm using Cytoscape to identify the key fundamental process modulated during infection. A total of ten clusters were identified among the upregulated genes of BCG-infected pulmospheres, whereas 36 clusters were identified among the genes of *M. tuberculosis*-infected pulmospheres. The top up-regulated cluster in the case of BCG infection was identified with an MCODE score of 19.8, whereas in the case of downregulated genes, 14 clusters were found with the highest score of 31.43 (Supplementary data 4). To investigate the biological and immunological behavior of the highly interconnected upregulated modules, we performed GO enrichment using ClueGo on the top two MCODE clusters shown in Supplementary Fig. 12A, and Supplementary Fig. 12B. Subsequently, ClueGo analysis reveals sterol biosynthetic process, isoprenoid biosynthetic process, cellular response to interleukin-1; and neutrophil migration, regulation of macrophage activation and positive regulation of type-2 immune responses were the major networks in the upregulated top two highly interconnected gene clusters during BCG infection (Supplementary Fig. 12C, D). Further, Cytohubba analysis reveals *HMGCR, HMGCS1, SQLE, FDT1, FDPS, MSMO1, CYP51A1, DHCR24, MVD*, and *LSS* are the key genes among all the upregulated genes in the case of BCG infected pulmospheres (Supplementary Fig. 12E).

Among 36 up-regulated critical network clusters in the case of the upregulated DEGs following *M. tuberculosis* infection, the highest MCODE score of 9.9. Among the 47 clusters identified in the case of the downregulated genes, the highest score was 81.3 (Supplementary data 5). Figure 7A, B depict the top two highly interconnected clusters. Functional analysis of these two clusters reveals extrinsic apoptotic signaling pathway, cellular response to IFN-γ, endothelial development, and antiviral response-related pathways in case of the cluster1 (Fig. 7C), and nucleoside

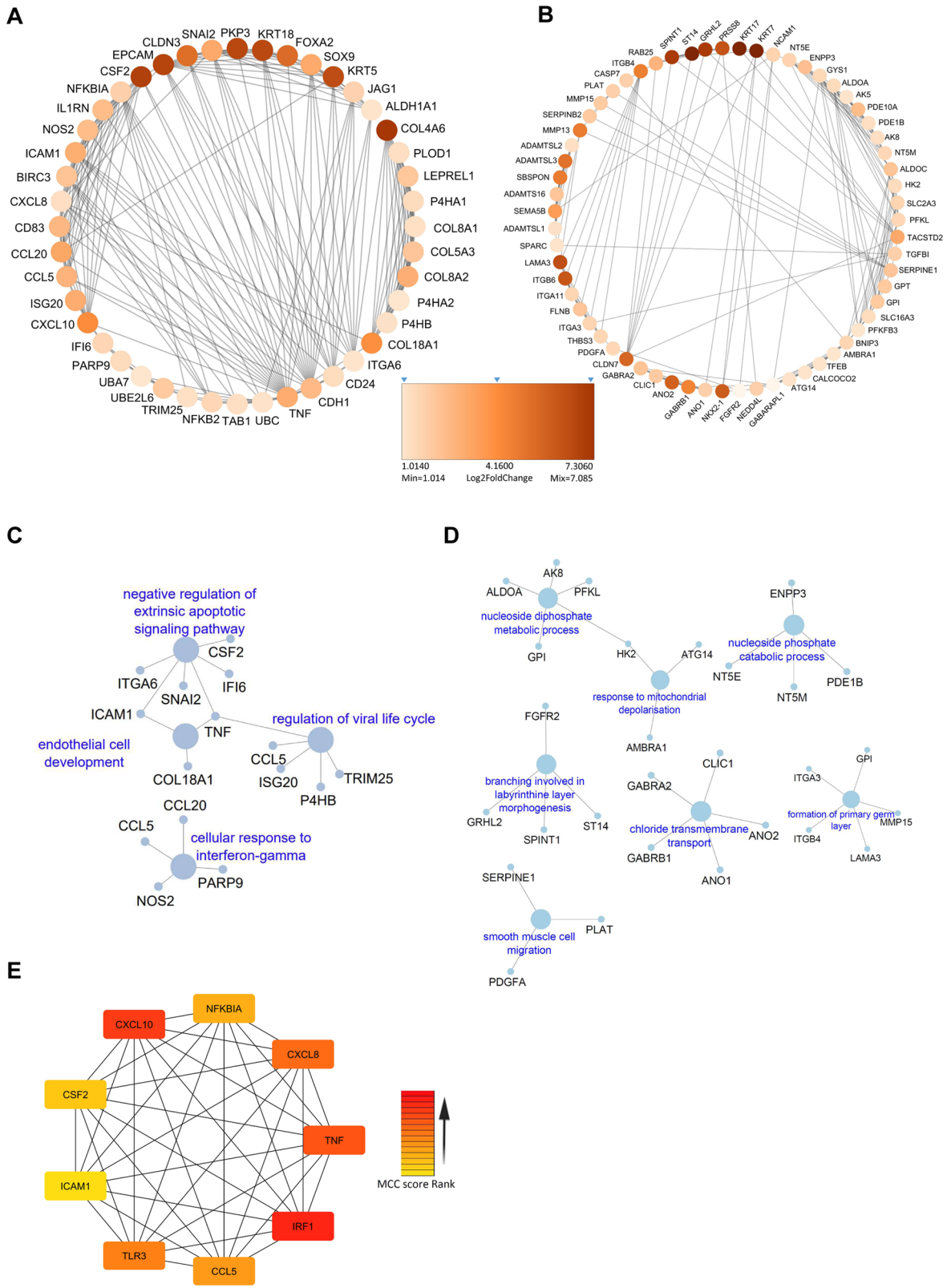

Fig. 7 | Network analysis of the up-regulated genes in *M.tuberculosis*-infected pulmospheres. Critical networks cluster1 (**A**) and cluster2 (**B**) were constructed using MCODE algorithm in Cytoscape. ClueGO based GO of biological process, and immune related pathways in highly interconnected cluster1 (**C**) and cluster2 (**D**). **E** Top relevant Hub genes identified in PPI network of DEGs in PS-*M. tb* using Cytohubba MCC-based method.

diphosphate metabolic process response to mitochondrial depolarization and smooth muscle migration in case of cluster2 were major upregulated networks in case of *M. tuberculosis* infection (Fig. 7D). Additionally, by using Cytohubba-based analysis of the total upregulated genes following *M. tuberculosis* infection we identified *CXCL8, CXCL10, CCL5, TNF, CSF2, ICAM1, TLR3, IRF1, and NF-kB1A* as major upregulated hub genes amongst the complex protein interaction networks (Fig. 7E). Notably, hub genes identified for *M. tuberculosis* infections are distinct from the BCG group. Hub genes are central to biological mechanisms and represent potential signatures for an ongoing infection or disease state.

Commonality and divergence of host responses to BCG and *M. tuberculosis* infection

Analysis of the DEGs identifies 388 common genes between BCG and *M. tuberculosis* groups, of which 307 showed a similar trend of either up or downregulation, and 81 genes exhibited inverse regulation (Fig. 8A).

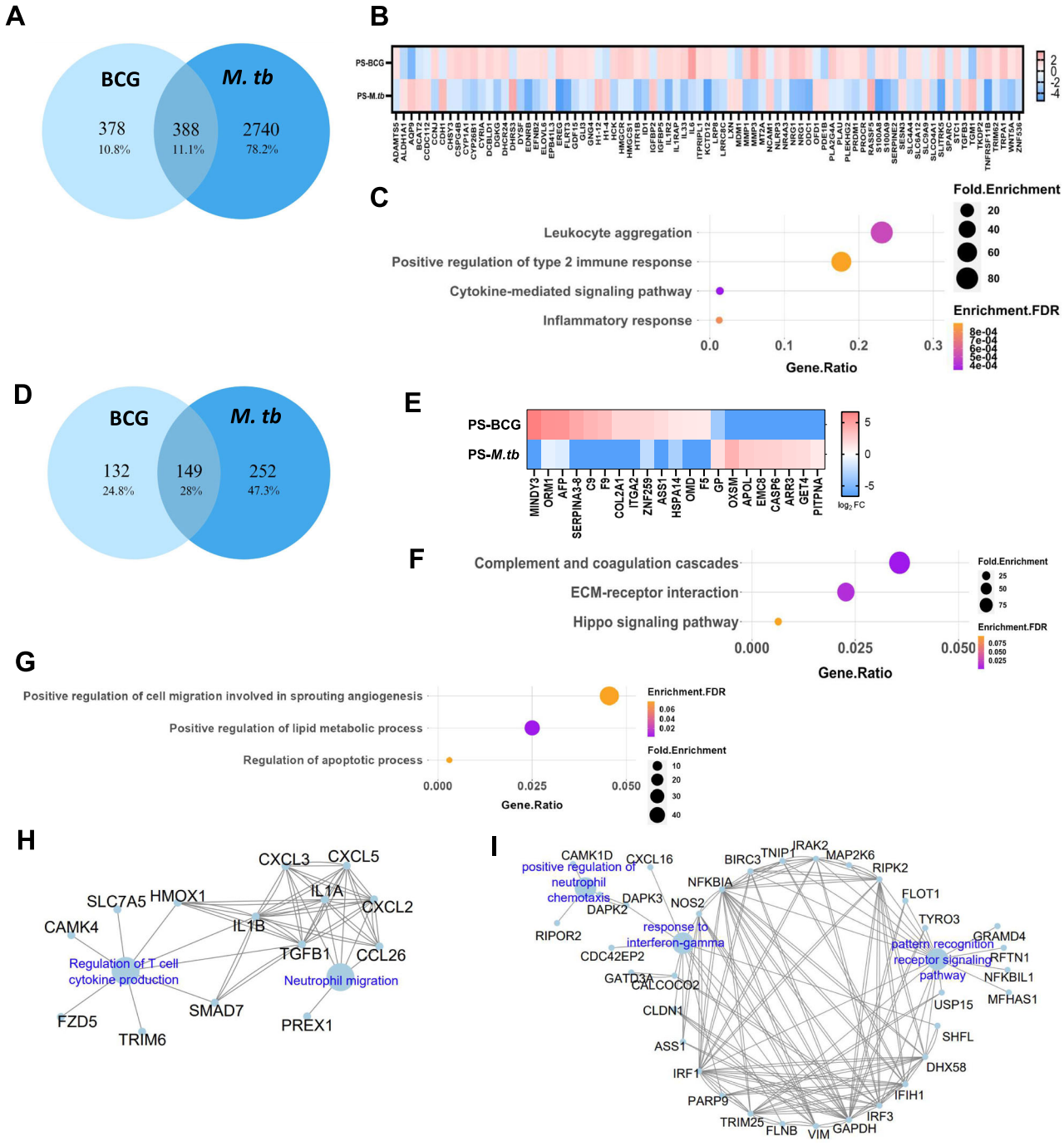

Fig. 8 | Divergence in the host responses to BCG and *M. tuberculosis* infection. **A** Venn diagram of DEGs shows common and unique genes upon BCG and *M.tb* infection of the pulmospheres. **B** Heat-map representing inversely regulated differentially expressed genes among common genes upon BCG and *M.tb* infection of the pulmospheres. **C** Top GO terms of common up-regulated genes in case of BCG infection and down regulated in *M.tb*. **D** Venn diagram of DEPs shows common and unique genes upon BCG and *M.tb* infection. **E** Heat-map representing the inversely regulated differentially expressed proteins upon BCG and *M.tb* infection. **F** Top GO terms of biological process for inversely regulated proteins that are upregulated in case if *M. tuberculosis* infection but down regulated in BCG infection. **G** Top GO terms of biological process up-regulated in case of BCG infection, but down regulated in case *M. tuberculosis* infection. **H** Immune network interaction that are up-regulated exclusively following BCG infection. **I** Immune network interaction upregulated exclusively upon *M. tuberculosis* infection.

Among the inversely regulated genes, 21 genes were upregulated and 59 were downregulated in *M. tuberculosis* compared to BCG infection (Fig. 8B). GO analysis of the genes that are upregulated in case of BCG infection identified highly relevant immune response-related biological processes and pathways (leukocyte aggregation, type-2 immune responses, and other cytokine signaling pathways) in case of BCG infection (Fig. 8C). Major genes involved in these immune response pathways were *HCK, WNT5A, IL1R2, IL1RAP, IL33, TRIM62, EREG, MT2A, IL6, MMP1, MMP3, LRP8*, and *TNFRSF11B* (Fig. 8B). On the contrary, these genes were significantly downregulated in the case of *M. tuberculosis* infection indicating the possibility that *M. tuberculosis* infection subverts certain immune responses in its favor, and limits tissue repair and remodeling process. Notable genes that were significantly upregulated in the case of *M. tuberculosis* infection but downregulated in the case of BCG infection are *RASSF5, CDH1, IGFBP2, TGFB3, and SPARC*. Genes such as *IGFBP2* and *TGFB3* are involved in immune processes, while *RASSF5* plays a role in apoptotic pathways, influencing host cell survival. Additionally, *CDH1* and *SPARC* may modulate cell adhesion mechanisms and tissue remodeling processes, potentially impacting M. *tuberculosis* entry and dissemination within the host.

Analysis of the DEPs identifies 149 common proteins between BCG and *M. tuberculosis* groups (Fig. 8D), of which 128 showed a similar trend of either up or downregulation, and 21 genes exhibited inverse regulation (Fig. 8E). GO analysis on the 21 inversely regulated proteins highlights complement and coagulation cascade pathways, ECM-receptor interaction, and Hippo signaling pathway involving 13 genes as critical signaling pathways that are upregulated in case of *M. tuberculosis* infection but downregulated in case of BCG infection (Fig. 8F). On the contrary, 8 genes belonging to cell migration and angiogenesis, lipid metabolism, and apoptosis were upregulated in the case of BCG infection, but downregulated in the case *M. tuberculosis* infection (Fig. 8G).

Analysis of the unique DEGs in the case of BCG infection identifies 233 genes upregulated and 145 genes downregulated (Fig. 8A). ClueGo-based immune responses related pathway analysis of the upregulated genes highlights neutrophil chemotaxis (*CXCL3, CXCL2, CXCL5, CCl26, PREX1, IL1A*, and *IL1B*) and regulation of T-cell cytokine production (*TGFB, SMAD7, HMOX1, CAMK4, TRIM6, SLC7A5*, and *FZD5*) as the significantly upregulated pathways (Fig. 8H). Whereas, *M. tuberculosis* infection resulted in 1258 up and 1482 downregulated genes, and ClueGO analysis reveals enrichment of leukocyte activation, differentiation, migration, TLR-3 signaling, and response to IFN-γ pathways among the leading upregulated pathways (Fig. 8I).

Integrated analysis of transcriptome and proteome data identified potential biomarkers for early *M. tuberculosis* infection in bovines

Integration of transcriptomics and proteomics data highlighted key gene/protein expression signatures for *M. tuberculosis* and *M. bovis* BCG infection in the bovine pulmospheres. Sixteen genes/proteins in the case of BCG infection, 82 genes/proteins in the case of *M. tuberculosis* infection, and 59 proteins/genes uniquely expressed in the case of *M. tuberculosis* infection over BCG infection at both transcriptional and proteomic level (Fig. 9A). Multi-gene correlation analysis reveals statistically significant positive correlation of 0.61 ($p = 0.015$), 0.52 ($p = 4.7e\text{-}07$), and 0.35 ($p = 0.0062$), respectively for the genes commonly regulated at both transcriptional and proteomic level (Fig. 9B). Next, by comparing the commonly upregulated genes/proteins from the three conditions discussed above (Fig. 9C–E), we sort-listed 15 genes (COL17A1, CFB, APOA1, S100A2, SERPINE1, RBP4, TNFAIP8, ASS1, ITGA3, GYS1, ASL, MTHFD2, CLU, USP15, FDT1) as unique transcriptomic/proteomic marker of *M. tuberculosis* infection.

In silico comparative analysis of potential *M. tuberculosis* infection biomarkers with published omics data

Nine hub genes identified from transcriptome data, and 15 upregulated genes, selected from the integrated analysis were chosen (24 genes) for further analysis for identifying potential markers of *M. tuberculosis* infection of the bovine lungs (Fig. 10A). These genes/proteins could have significant potential as biomarkers for TB disease diagnosis, treatment monitoring, and the evaluation of vaccine-induced responses. We employed a robust in silico validation protocol to evaluate the cohort of identified genes. This involves a meticulous comparison with publicly available TB-transcriptome datasets (23 independent studies were included). The criteria for the selection of this dataset were described in detail in the materials and method section. Figure 10B illustrates the transcriptional status of selected 24 genes across all the data sets. Remarkably, 12 genes (IRF1, CXCL10, TNF, CXCL8, CCL5, ICAM1, COL17A1, CFB, SERPINE1, TNFAIP8, MTHFD2, and USP15) were found to be represented in more than 50% of the datasets. Finally, using a minimum cut-off Log2 fold induction of 0.585 (>1.5 fold in linear scale), and careful consideration of the nature of the bio-molecules, we shortlisted six genes/protein (IRF1, CXCL8, CXCL10, CCL5, SERPINE1, and CFB) as potential *M. tuberculosis* early infection biomarker (Fig. 10C).

Further, considering the relevance of animal lineage MTBC species, such as *M. bovis* and *M. orygis* in cattle TB incidences, we evaluated the selected markers using real-time PCR-based gene expression analysis. Pulmospheres were infected with virulent *M. bovis* AN5, *M. orygis* NIAB1 strains[33], and *M. tuberculosis* H37Rv. A significant upregulation of majority of the selected genes was observed (>1.5 fold, $p > 0.05$), with distinct expression patterns across *M. tuberculosis, M. bovis, and M. orygis*, highlighting pathogen-specific immune responses (Fig. 10D). Notably, the fold upregulation of CCL5 (>40 fold), IRF1 (>25 fold), CXCL10 (>600 fold), and CXCL8 (>600 fold) was significantly higher in *M. tuberculosis* infection compared to the fold upregulation of these genes in case of animal lineage *M. bovis* and *M. orygis* infection. Conversely, *CFB, and SERPINE1* show no distinct expression pattern between human, and animal lineage mycobacterial infections, indicating their limited utility as lineage-discriminatory markers. In case of *M. bovis* infection, only *SERPINE1* (>10 fold) and *CXCL8* (>30 fold) exhibited moderate upregulation, while other genes exhibited nominal changes. In contrast, *M. orygis* infection resulted in a markedly higher expression of *CCL5* (>8 fold), *CFB* (>6 fold), *IRF1* (>6 fold), *CXCL10* (>130 fold), and *CXCL8* (>30 fold). These findings suggest that while a core upregulated gene signature is shared across the three MTBC species, the magnitude of host responses varies in a pathogen-specific manner.

Discussion

In pursuit of a comprehensive understanding of bovine pulmonary TB, and the intricate host responses, this study undertakes the development of a robust and reproducible ex vivo disease model. The primary objective herein is to establish an innovative 3D pulmosphere model that recapitulates bovine TB and elucidates the fundamental signaling pathways and pivotal genes/proteins implicated in host-pathogen interaction during the early phase of TB infection within the bovine lungs. Notably, our 3D pulmosphere model fosters the co-culture of diverse cell types, encompassing macrophages, epithelial cells, fibroblasts, alveolar cells, and other immune cells intricately interconnected by the lung's extracellular matrix components. This advancement stands in marked contrast to conventional 2D cell cultures, which frequently fail to replicate the cellular heterogeneity, and complexity of multicellular interactions. With its higher ability to model TB infection within the lungs, the 3D pulmosphere model holds promise for deepening our insights into the bovine TB disease and facilitating the discovery of novel diagnostic biomarkers and therapeutic targets.

The long-term cultivability of multicellular spheroids over 21 days provides a significant advantage for studying slow-growing bacteria like *M. tuberculosis*. This allows for a more comprehensive analysis of host-pathogen interactions, capturing the prolonged dynamics of infection and immune response, which is not achievable in standard macrophage 2D cultures. The dynamic nature of cell viability, hypoxia and ROS levels varying across different depths within the 3D pulmospheres underscore a key advantage over traditional 2D cultures. This spatial variability closely resembles in vivo granuloma microenvironments, wherein central necrosis, cell death, and hypoxia are some of the key features, offering a more

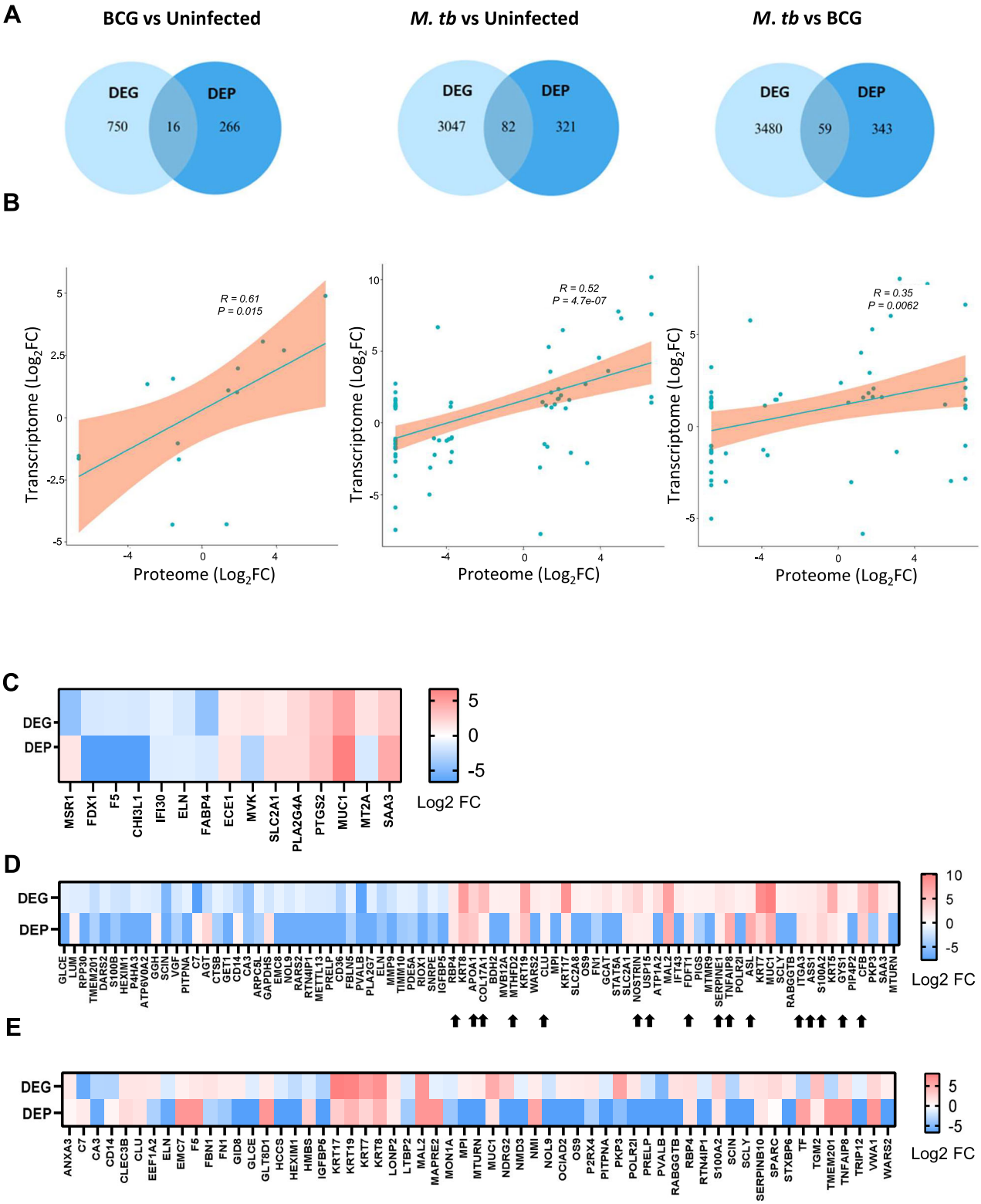

Fig. 9 | Integrated analyses of transcriptome and proteome data identify key markers of *M. tuberculosis* infection. **A** Venn diagram of DEGs and DEPs shows common and unique genes/proteins upon BCG and *M. tuberculosis* infection. **B** Correlation between Log_2FC of transcriptome and proteome data for the common genes. *P* value < 0.05. **C** Heatmap representing the Log2 FC of DEGs and DEPs upon BCG vs uninfected. **D** Heatmap representing the Log2 FC of DEGs and DEPs upon *M. tuberculosis vs* uninfected. **E** Heatmap representing the Log2 FC of DEGs and DEPs upon *M. tuberculosis* infection vs BCG infection.

physiologically relevant platform for studying *M. tuberculosis* host-pathogen interactions within the lung in more realistic manner.

Our investigation employing the 3D pulmosphere uncovered distinctive immunological pathways that distinguish between the responses induced by vaccine strain BCG and the virulent strain *M. tuberculosis*. Notably, *M. tuberculosis* infection precipitated a heightened divergence in gene expression and pathway regulation, accompanied by unique cellular signaling as compared to BCG infection. This divergence was evident in the

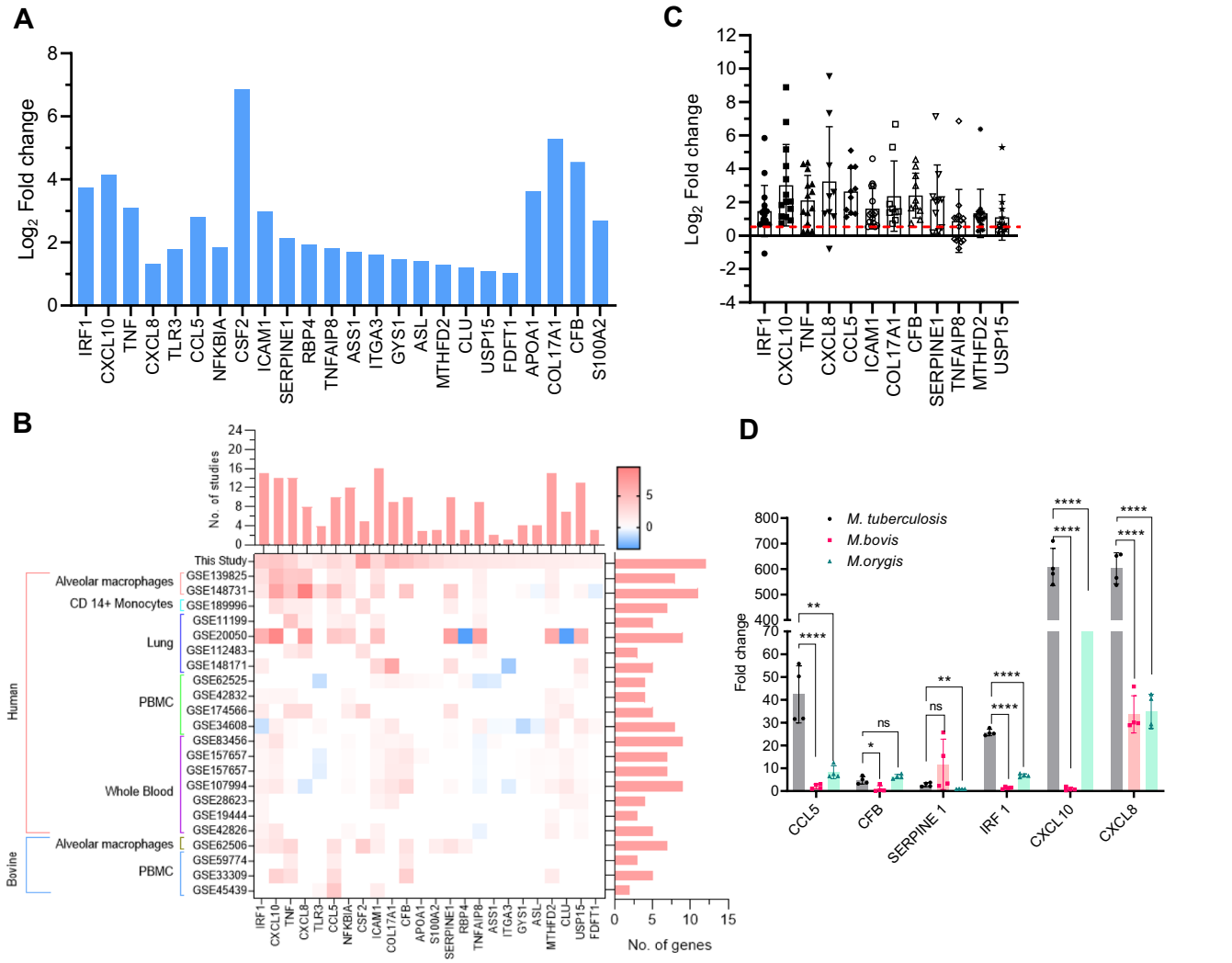

Fig. 10 | Potential biomarkers of early *M. tuberculosis* infection, and comparison with published omics data. A Bar diagram illustrates the Log2 fold change of 24 key genes selected in this study. **B** Heat-map represents the Log2 fold change of the key genes across selected similar omics studies, the bar diagram above the heat-map depicts the number of studies with upregulation of the specific gene, and the bar diagram on the right side of the heat map shows number of genes detected in a selected study. **C** The dot plot with mean and SD graph represents the Log2 fold change values of each gene across all 23 selected studies. The red dashed line denotes the applied cut-off Log2 fold value of 0.585 (1.5-fold in linear scale). **D** Comparative gene expression analysis of *M. tuberculosis, M. bovis*, and *M. orygis* pulmospheres using Real-Time PCR. Individual data points in the bar graph represent fold gene expression in each biological replicate ($n = 4$). Data information: Statistical analysis included an unpaired two-tailed *t*-test for comparison between two. Error bar is mean ± SD, $n = 4$, *, $P < 0.05$; **, $P < 0.01$; ****, $P < 0.0001$.

heightened activity of the genes of complement and coagulation cascades and ECM receptor interactions within the 3D microenvironment of *M. tuberculosis*-infected pulmospheres, in contrast to BCG-infected pulmospheres. On the other hand, positive regulation of cell migration, lipid metabolism, and apoptotic process were the top up-regulated pathways following BCG infection, which corroborates previous findings[34,35].

Further, a noteworthy finding: the heightened expression of interferon-stimulated genes and interferon regulatory factor (IRF) genes associated with both type-1 and type-2 interferon pathways during the initial phase of TB infection. While the important role of IFN-γ (type-2 interferon) in human TB is well known, the role of the Type-1 IFN pathway is conflicting, with some studies indicating its promotion of pathogen-favouring host responses and others suggesting the opposite[36–39]. However, its role in modulating TB disease in bovine hosts remains largely unexplored. In a precision-cut lung slice model, the Type-1 IFN pathway was found to be highly upregulated in the case of *M. bovis* infection compared to *M. tuberculosis* infection[15]. Our bovine 3D pulmosphere model highlights type-1 IFN pathway as one of the leading pathways during early infection of bovine lungs with the tubercle bacilli.

Intriguingly, our investigation highlights an upregulation of the Th17 signaling pathway following exposure to BCG. Activation of the Rap1 pathway following BCG vaccination leads to heightened production of IL-17, a pivotal cytokine in combating mycobacterial infections[40]. Noteworthy evidence supports the induction of the IL-17 pathway following BCG vaccination, fostering protective immunity against *M. tuberculosis* in animal models[41]. Interestingly, *M. tuberculosis* infection also leads to IL-17 production in our study, however, at a comparatively subdued level than BCG stimulation.

The interplay between BCG vaccination, *M. tuberculosis* infection, and TNF-α signaling has been well documented in both animal models and humans[42]. Our bovine pulmosphere model, has revealed a robust TNF signaling pathway activation following infection with both *M. bovis* BCG and *M. tuberculosis*. Notably, the response was more pronounced in the case of the latter. TNF-α holds a pivotal role in the protective immune response against mycobacteria and is instrumental in the formation of granulomas, a hallmark of TB disease[42,43]. BCG vaccination-induced TNF-α production proves indispensable for macrophage activation and mycobacterial eradication[44]. However, a delicate balance is necessary, as excessive TNF-α

production can trigger tissue damage and inadvertently exacerbate disease progression[45]. The 3D-pulmosphere model highlights its potential as a useful model to study TNF signaling in TB and therapeutic interventions targeting this critical pathway.

The heightened expression of the Advanced Glycation End-products (AGE) and Receptor for AGE (RAGE) pathway (AGE-RAGE) has been observed in *M. tuberculosis*-infected pulmospheres, highlighting its relevance in TB pathogenesis[46,47]. The formation of AGEs through non-enzymatic glycation of proteins and lipids is linked to inflammation and oxidative stress in diverse tissues. The Receptor for AGEs (RAGE), present on immune cells, becomes activated upon interaction with AGEs, initiating signaling cascades including NF-kB and MAPKs, and subsequently leading to the production of pro-inflammatory cytokines and chemokines[48]. In the case of idiopathic pulmonary fibrosis, the AGE-RAGE pathway emerges as a key contributor to lung damage, fibrosis, and granuloma formation[49]. Our finding underscores the AGE-RAGE pathway's role in bovine TB pathogenesis.

Significant perturbations in signaling pathways also encompass the Peroxisome proliferator-activated receptor (PPAR) pathway, notably upregulated in both BCG and *M. tuberculosis*-infected pulmospheres in this study. This pathway assumes a pivotal role in regulating lipid metabolism and immune responses[50]. In the context of TB, PPAR signaling emerges as a critical modulator of host immune responses to *M. tuberculosis* infection[51]. Notably, BCG vaccination can activate the PPAR signaling pathway, subsequently influencing the expression of genes pivotal to lipid metabolism and immune responses[34].

The in silico analysis of published OMICS data, combined with our experimental findings, highlights six genes/proteins- IRF1, CCL5, CXCL8, CXCL10, SERPINE1, and CFB as potential early biomarkers for *M. tuberculosis* infection in bovine pulmospheres. These markers have been previously implicated in various aspects of TB pathogenesis: IRF1 and CXCL10 in human active TB[52,53], CXCL8 and CCL5 in active and latent TB[54,55], and SERPINE1 in lung infections and inflammatory modulation[56,57]. Notably, our finding indicate CFB as a potential marker for early *M. tuberculosis* infection in the bovines which was previously identified as a biomarker for pancreatic ductal adenocarcinoma[58]. Additionally, findings of CXCL10 as an early TB biomarker resonate with a prior investigation that identified CXCL10 as a potential cell-mediated immuno-biomarker for bovine TB diagnosis[59]. Although our infection model utilized *M. tuberculosis* H37Rv, a strain reported to be attenuated in bovines compared to most other *M. tuberculosis* strains and *M. bovis*[23,24], the early infection gene signature derived from this study is consistent with findings from studies using virulent M. bovis as the infecting pathogen[9,13,30,60]. Further validation of this six-gene signature through real-time PCR following infection with virulent *M. bovis* and *M. orygis* in bovine pulmospheres reinforces the existence of a core upregulated gene set shared across multiple MTBC species. However, lineage- and pathogen-specific differences in the magnitude of host responses highlight the need for further investigation into the distinct immune dynamics triggered by different MTBC pathogens. Hence, further clinical validation is required to establish the diagnostic and clinical significance of the early infection gene signature in bovine TB.

The ex vivo bovine pulmosphere model offers an ethical alternative to live animal experiments by utilizing lung tissue from slaughterhouses. This model addresses challenges in studying early TB pathophysiology in bovine lungs, which are limited by the complexities of conducting experimental infections in large animals. The pulmosphere model enables high-throughput screening of TB drugs, allowing simultaneous evaluation of multiple candidates in a cost-effective and efficient manner. This serves as an intermediate platform before animal-based testing, facilitating the identification of drug targets and bacterial virulence factors.

While our 3D pulmosphere model offers versatile utility, it is important to acknowledge certain limitations that warrant further improvement and refinement. Creating and maintaining the 3D pulmosphere model presents greater challenges compared to traditional 2D cell culture, potentially constraining its adoption in certain laboratories[61]. Furthermore, the model's ability to replicate the intricate in vivo environment is not exhaustive, as it lacks the natural recruitment of immune cells from peripheral sites to the infection foci post-infection. Addressing this limitation could involve integrating relevant peripheral blood mononuclear cell (PBMC)-derived immune cells with lung-derived cells for pulmosphere generation and maintenance longitudinally over the course of infection. A key limitation of this study is the use of *M. tuberculosis* H37Rv, a human-adapted strain known to be attenuated in bovine infection, as the primary infecting strain. Although we validated gene signatures via real-time PCR following infection with virulent *M. bovis* and *M. orygis*, a more comprehensive transcriptomic and proteomic analysis using these animal-lineage strains is warranted to gain deeper insights into strain-specific host responses. Additionally, it's noteworthy that this study focused solely on host responses at the 24-hour post-infection mark; investigating responses during different phases of TB infection and granuloma formation using this model could enhance our comprehension of bovine TB pathogenesis and consequently refine intervention strategies. Further investigations must be conducted to confirm the functional significance of the identified genes and pathways in the pathogenesis of bovine TB. Notwithstanding these considerations, our findings offer valuable insights into the biological pathways and molecular mechanisms governing the bovine host's response to BCG and *M. tuberculosis* infections at the primary site of infection.

In summary, to the best of our knowledge, this is the first report demonstrating the development of an ex vivo 3D pulmosphere bovine TB model. The combination of diverse cell types and increased ECM-related protein expression in 3D pulmospheres emphasizes their relevance in studying host-pathogen interactions beyond 2D cultures. Transcriptomic and proteomic analyses provide a comprehensive view of the early host response to *M. tuberculosis* in bovine 3D pulmospheres, revealing species-specific responses, hub genes, and functional clusters. These findings offer new insights into the molecular mechanisms governing host–pathogen interactions during *M. tuberculosis* infection in the bovines, with potential implications for the discovery of disease biomarkers, host-directed therapies, and enhancing our understanding of TB pathogenesis, and ultimately aiding in the discovery of improved prevention and management strategies.

Methods

Ethics statement

All experiments were reviewed and approved by the Institutional Biological Safety Committee (IBSC, approval no. IBSC/2018/NIAB/BD/001) of the National Institute of Animal Biotechnology, Hyderabad, and animal experiments were approved by the Animal Ethics Committee of the West Bengal University of Animal and Fishery Sciences, Kolkata, India (Approval No. IAEC/22-B, CPCSEA Reg. No.763/GO/Re/SL/03/CPCSEA), and the Committee for the Purpose of Control and Supervision on Experiments on Animals, India. We have complied with all relevant ethical regulations for animal use.

Lung tissue and single-cell suspension preparation

The lung tissues used for deriving the 3D pulmospheres were obtained from crossbred Sahiwal × Holstein Friesian cattle (*Bos indicus* × *Bos taurus*). These animals were sourced from a government-approved abattoir, where they underwent thorough clinical and post-mortem inspection by certified veterinarians. To ensure the inclusion of only mycobacteria-naive and healthy animals, post-mortem lung tissue samples were carefully inspected for any pathological lesions. Additionally, a section of the same lung tissue was subjected to PCR-based evaluation for MTBC pathogens and non-tuberculous mycobacteria (NTM). Only tissues that tested negative for all mycobacterial DNA were included in the study. After thorough washing in PBS, the tissue was chopped into small pieces of approximately 2 mm × 2 mm size and kept in 5 ml DPBS containing liberase enzyme (5 mg in 1 ml/1 g of tissue) and was incubated at 37 °C in a 50 ml falcon tube for 40 min with intermittent agitation (every 10 mins). Following liberase treatment, 5 ml of DMEM complete media containing 1x HPES, 10% FBS was added and shaken vigorously to disassociate the tissue. The dissociated

cells were filtered through a 100-µm filter and pelleted at 1500 rpm for 5 min at room temperature (RT). Subsequently, cells were washed with DPBS, and red blood cell (RBC) lysis was performed using RBC Lysis Buffer™. Cells were then washed twice with DPBS, followed by DMEM complete media, and finally resuspended in DMEM-F12 complete media (consisting of 10% FBS, 1X Antibiotic–Antimycotic solution). Cells were seeded into a T-25 flask grown for 7 days, and subsequently used for pulmosphere preparation.

Preparation of poly-HEMA-coated plates

For a generation of 3D pulmospheres, poly-HEMA coated plates were used[18]. Briefly, Poly 2-hydroxyethyl methacrylate (poly-HEMA) stock solution was prepared (120 mg/ml) in 95% ethanol by dissolving the crystals at 65 °C on a heat block for 10–12 h. The working solution of poly-HEMA (5 mg/ml) was prepared by vortexing briefly for 30 s, and added into 96-well U-bottom plates (160-µl/well). Plates were left at RT in a sterile laminar hood for 24 h until the plates were fully dry. These coated plates were used for the preparation of the pulmospheres.

Preparation of the pulmosphere

Seven days cultured primary lung cells were detached from the T-25 flask using trypsin (0.5%) and neutralized with 5 ml DMEM complete media. Cells were collected by centrifugation at 300 *g* for 5 min at RT. The cell pellet was resuspended in a 2 ml complete DMEM medium, and cell viability and live cell density were measured via the trypan blue exclusion method. Subsequently, 8000–10,000 cells were added per well in the poly-HEMA–coated 96-well U-bottom plates. The plate was centrifuged at 200 *g* at RT for 1 min and was incubated for 24 h at 37 °C and 5% CO_2 in a TC incubator resulting in the formation of spheroids. These multicellular 3D-spheroids derived from the primary lung cells were termed "pulmospheres". Pulmospheres were derived from three animals per experimental group. From each animal, at least 10 pulmospheres were included for analysis in each group. This experimental design allowed us to capture biological replicates and assess individual animal variations in host responses. The day-wise growth of pulmosphere was measured using image J and motic image plus 3.0 software.

Assessment of live and dead cells in pulmospheres

Pulmospheres were subjected to live-dead staining to assess cell viability. CFSE (carboxyfluorescein succinimidyl ester) was used to stain live and proliferating cells, while propidium iodide (PI) was employed to label dead cells. Following cultivation, the pulmospheres were washed twice with DPBS to remove residual media and incubated in DPBS containing CFSE and PI, both diluted to a final concentration of 1:1000 as per the manufacturer's instructions. The stained pulmospheres were visualized using confocal and wide-field fluorescence microscopy. Live cells were identified by CFSE fluorescence (excitation/emission: 490/525 nm), and dead cells were marked by PI fluorescence (excitation/emission: 596/670 nm), enabling a precise evaluation of cell viability within the pulmospheres.

Assessment of hypoxia and oxidative stress in pulmospheres

Hypoxia and ROS levels in the pulmospheres were assessed using the ROS-ID® Hypoxia/Oxidative Stress Detection Kit (Enzo Life Sciences, Inc., New York, USA), which includes fluorescent probes specific for hypoxia (red fluorescence) and ROS (green fluorescence). Pulmospheres were cultured in DMEM complete media and incubated at 37 °C in a humidified atmosphere (95% humidity, 5% CO_2). At specific time points (Day 1, Day 7, Day 14, and Day 21), the DMEM media was removed, and the pulmospheres were washed twice with DPBS to eliminate residual media. Subsequently, they were incubated in DPBS containing the fluorescent probes. Fluorescent probes were diluted and prepared according to the manufacturer's protocol. After staining, the pulmospheres were visualized using a wide-field fluorescence microscope equipped with fluorescein (490/525 nm) and Texas Red (596/670 nm) filters, enabling detailed analysis of temporal changes in hypoxia and ROS levels.

Microscopy and image acquisition

Images of the pulmospheres were captured using multimodal microscopes and applications including, bright field, fluorescence, confocal, live cell imager as well as super-resolution microscopy, as and when applicable as mentioned in the figure legends. For acquisition and analysis of the fluorescence data, Z-stacking for each image began at the initial detection of fluorescence across different channels and concluded at the point of diminished intensity. Maximum intensity projections were generated from each stack and utilized for signal intensity calculations. Three-dimensional (3D) and 2.5-dimensional (2.5D) images/movies were constructed by merging all z-stacks. Analysis, deconvolution, and image construction were performed using Zen Pro (Blue Edition) and ImageJ software.

Mycobacterial cultures

The *Mycobacterium bovis* BCG (Danish 1331 strain) and *M. tuberculosis* (H37Rv strain) were cultured in Middle Brook (MB) 7H9 broth containing 1x Oleic Acid Dextrose Catalase supplement and 0.02% Tween 80 following standard method[62]. Bacteria from the mid-log phase broth culture were used for the preparation of glycerol stocks and stored at −80 °C for subsequent use. For the in vitro infection, fresh bacterial cultures were grown from the glycerol stock to the mid-log phase, washed thoroughly with 1X PBS, and resuspended in DMEM incomplete media (without FBS and antibiotic-antimycotic mix) for use in the infection experiment.

Bovine pulmosphere TB infection model

To establish the 3D-pulmosphere *M. tuberculosis* infection model, cultured primary lung cells from passage number 0 or 1 were infected with the tubercle bacilli from logarithmic phase bacterial culture at a pre-calibrated MOI of 1:10 (cell:bacteria). Following three hours of infection cells were thoroughly washed to remove the extracellular bacteria. Cells were then detached from the 2D culture using trypsin (0.5%) and single cell suspension of infected mixed cells was used for the formation of *M. tuberculosis*-infected 3D pulmosphere using the same method described in the above sub-section "Preparation of the pulmosphere". Additionally, *M. bovis* BCG was also used to generate BCG-infected 3D-pulmopheres following the same protocol.

Sample preparation for mass spectrometry

For the preparation of each sample for mass spectrometry (MS) analysis, ten pulmospheres from each treatment group were pooled containing ~1×10^5 cells, and lysis was performed using lysis buffer containing 2% Sodium deoxycholate (SDC) in 50 mM Tris HCL (PH 7.5). Protein concentrations were measured by Bradford assay. The protein samples were treated with dithiothreitol at 57 °C for 1 h to reduce disulfide bonds and subsequently alkylated by iodoacetamide treatment for 1 h in the dark at RT. Then samples were subjected to trypsin digestion overnight at 37 °C at a ratio of 1:20 (trypsin:protein) followed by SDC separation via formic acid (25%) treatment. Digested protein samples were then filtered through a 10 kDa membrane filter to remove undigested proteins followed by salt removal using the C18 column and samples were vacuum dried. Finally, the dried samples were reconstituted in 0.3% formic acid, quantified using a spectrophotometer, and 1 µg of peptide samples were subjected to tandem MS–MS analysis.

Mass spectrometry data acquisition and data analysis

The Ultimate 3000 RSLCnano system coupled with the high-resolution Q Exactive HF mass spectrometer (Thermo Fisher) was used. The full MS1 scans were set with a resolution of 60,000 ions, an automatic gaining control (AGC) target value of 1×10^6, and an acquisition range of 375–1600 m/z with a 60 ms maximum injection time. For the fragmentation, the top 25 precursors were selected. For the MS2 acquisition, a resolution of 15,000 ions, a target AGC value of 1×10^5, with a maximum injection time of 100 ms, an isolation window of 1.3 m/z, and a fixed first mass at 100 m/z were specified. Peptide elution was performed with a

nonlinear gradient flow of 0.300 µL/min during 180 min using 5% of solvent B (80% acetonitrile + 0.1% formic acid) and 95% of solvent A (0.1% formic acid). The data was analyzed using proteome discoverer v2.5 (Thermo Fisher).

RNA extraction from the pulmosphere

RNA isolation was performed using a combination of trizol (sigma) and RNeasy Mini plus Kit (Qiagen). Briefly, 1 ml trizol was added to the pooled pulmospheres samples, vortex vigorously and 200 µL chloroform was added. Samples were then shaken for 15 s, incubated for 3 min at RT, and then centrifuged at 12,000 *g* for 15 min at 4 °C. The upper aqueous layer was separated and proceeded further for RNA extraction using RNeasy Mini kit following manufacturer's instructions. Total RNA was eluted with 30 µL RNase-free H_2O and stored at −80 °C. the RNA concentration and purity were checked using Nanodrop 1000 (Thermo Fisher).

Whole transcriptome sequencing and analysis

RNA quantity is checked with Qubit fluorometer (Thermofisher #Q33238) using RNA HS assay kit (Thermofisher #Q32851) following manufacturer's protocol, and subsequently, RIN values were estimated in a tapestation 4150 using HS RNA screen tape (Thermo Fisher). The library preparation was carried out using TruSeq® Stranded Total RNA kit (Illumina #15032618, Illumina #20020596). Final libraries were quantified using Qubit 4.0 fluorometer (Thermofisher #Q33238) using a DNA HS assay kit (Thermofisher #Q32851) following the manufacturer's protocol. To identify the insert size of the library, we queried it on Tapestation 4150 (Agilent) utilizing highly sensitive D1000 screentape (Agilent # 5067-5582) following manufacturers' protocol. Quality assessment of the raw fastq reads of the sample was performed using FastQC v.0.11.9 (default parameters)[63]. The raw fastq reads were preprocessed using Fastp v.0.20.1 (parameters: --trim_front1 9 --trim_front2 9 --length_required 50 –correction --trim_poly_g --qualified_quality_phred 30)[64], followed by quality re-assessment using FastQC and summarization using MultiQC[65]. The processed reads were aligned to the STAR indexed Bos taurus ARS-UCD1.2 genome using STAR aligner v 2.7.9a (parameters: "--outSAMtype" BAM SortedByCoordinate, "--outSAMunmapped" Within, "--quantMode", TranscriptomeSAM, "--outSAMattributes" Standard) *Bos Taurus* (ARS-UCD1.2)[66]. The rRNA features were removed from the GTF file of Bos taurus genome ARS-UCD1.2. The alignment file (sorted BAM) from individual samples was quantified using featureCounts v. 0.46.1 based on the rRNA-filtered GTF file to obtain gene counts[67]. These gene counts were used as inputs to DESeq2 for differential expression estimation (parameters: threshold of statistical significance --alpha 0.05; *p*-value adjustment method: BH)[68]. For Gene Ontology (GO) and Kyoto Encyclopedia of Genes and Genomes (KEGG) Pathway annotation, the up and down-regulated gene IDs were extracted from the DESeq2 result files and subjected to bioDBnet[69]. ShinyGO 0.77 was used for functional enrichment analysis, and cross-verified with g:Profiler. Venn diagrams were produced using Venny 2.1. Heatmaps were generated following hierarchical clustering, and discriminating variables between comparison groups were identified using a false discovery rate of $p < 0.005$ or $q < 0.2$.

Network analysis

Upregulated and downregulated genes from proteome and transcriptome were used to construct protein–protein interaction network (PPI) using Online Database STRING. Full string network types having both physical and functional association with medium confidence 0.4 were kept as default settings. The resultant network was imported to Cytoscape software (3.9.1) to analyze the PPI network[70]. Highly connected clusters were identified using MCODE clustering method. The highest MCODE score in the network was subjected to GO enrichment analysis using ClueGO setting a two-sided hypergeometric test with Bonferroni step-down corrected p-value ≤ 0.05, and kappa score ≥0.4 as statistical parameters. The maximal clique centrality (MCC) method was applied to identify the important hub genes based on the MCC Score[71].

In silico comparative analysis for validation of *M. tuberculosis* infection signature

We implemented a rigorous validation protocol to assess a set of identified genes that potentially serve as key regulators in bovine tuberculosis (TB) conditions. To validate these key genes, we compared them against publicly available TB infection transcriptome datasets. We specifically focused on multiple TB disease cohort studies accessible through the NCBI Gene Expression Omnibus (GEO) database (https://www.ncbi.nlm.nih.gov/geo/). The list of selected studies, along with their GEO accession numbers, is provided in Supplementary data 6. Our selection criteria were confined to two species: Bovine and Human. We used search terms such as "Bovine tuberculosis host transcriptomic", "Bovine tuberculosis RNA seq", "Tuberculosis lung transcriptome", "Tuberculosis blood signature", "Tuberculosis lung signature", "Tuberculosis host RNA seq", "Tuberculosis PBMC gene expression", "Tuberculosis whole blood gene expression", "Tuberculosis lung gene expression", and "Tuberculosis sputum". These terms encompassed both microarray and high-throughput sequencing data types. The dataset inclusion criteria encompassed studies involving *M. tuberculosis* and *M. bovis* infections specifically in peripheral blood mononuclear cells (PBMC), whole blood, lung, and alveolar macrophages (AM). In broad terms, the analyses centered around comparing groups infected with *M. tuberculosis* and *M. bovis* with their respective healthy control groups. Based on the above inclusion factors 22 studies were considered for further comparison. The identification of DEGs was performed using GEO2R, integrated with the limma package, considering genes with statistically significant differences between pairwise groups (adjusted P value < 0.05, FDR < 0.05).

Real-time PCR

The PrimeScript First Strand cDNA Synthesis Kit (Takara) was employed to synthesize cDNA from RNA, adhering to the manufacturer's protocol. Both random hexamer primers and oligo(dT) primers were used in the reaction. Primers targeting bovine genes (CCL5, CFB, SERPINE1, IRF1, CXCL10, CXCL8, and ICAM1) were designed via Primer-BLAST (NCBI). Quantitative real-time PCR (qRT-PCR) was performed on a CFX96 Touch System (Bio-Rad). Primer sequences are listed in (Supplementary Table 1). The PCR conditions included an initial denaturation at 95 °C for 2 min, followed by 40 cycles of denaturation at 95 °C for 15 s and annealing/extension at 55–65 °C for one minute, depending on the target gene. A melt curve analysis was conducted by increasing the temperature in 0.5 °C intervals from 65 °C to 95 °C, with fluorescence being recorded throughout the process. The 2^−ΔΔCT method was used for calculating the relative gene expression, with RPLP0 as the reference.

Statistics and reproducibility

The statistical analysis for this study was conducted using a combination of bioinformatics tools and statistical software, with details provided in the figure legends or relevant subsections within the "Materials and Methods" section. Differential gene/protein expression was considered significant if the false discovery rate (FDR) was below 0.05 and the log2 fold change exceeded ±1. DESeq2 was employed for differential expression analysis, while principal component analysis (PCA) was used to assess sample variance and clustering. To visualize differentially expressed genes/proteins and their expression patterns, volcano plots and heatmaps were generated. Enrichment analysis for GO terms and pathways was performed using a hypergeometric test, with statistical significance set at a p-value < 0.05. Data visualization and statistical evaluations were primarily conducted in R (version 4.3.2). GraphPad Prism 9 software (GraphPad, CA, USA) was also used in specific instances, wherein statistical analysis included an unpaired two-tailed t-test for comparison between two groups, and data are presented as mean ± sd unless otherwise specified in the figure captions. A 95% confidence interval or 0.05 threshold for significance ($p < 0.05$) was used in all statistical tests. For correlation analysis, GraphBio was used[72]. To guarantee biological reproducibility, each experiment included a minimum of three biological replicates. Additionally, variability analysis of selected omics

data was performed to confirm the consistency and relatedness of samples within each experimental group.

Databases used for analysis

Several publicly available databases were used to aid in the in-depth analysis of cell types, networks, and pathways based on the transcriptome and proteome data. Some of the major databases include Matrisome DB for ECM atlas[27]. All the databases and software information are provided in the Supplementary data 7.

Reporting summary

Further information on research design is available in the Nature Portfolio Reporting Summary linked to this article.

Data availability

All transcriptome and proteome data are available in the NCBI GEO accession number GSE246765, and in ProteomeXchange consortium via PRIDE [96] partner repository with the database identifier PXD046641, respectively. Numerical source data of graphs/charts presented in the main figures are provided as Supplementary data 1-8. All other data supporting the findings of this study are available from the corresponding author upon reasonable request.

Received: 17 April 2024; Accepted: 4 March 2025;
Published online: 04 April 2025

References

1. Borham, M. et al. Review on bovine tuberculosis: an emerging disease associated with multidrug-resistant mycobacterium species. *Pathogens* **11**, 715 (2022).
2. Kock, R. et al. Zoonotic tuberculosis—the changing landscape. *Int. J. Infect. Dis.* **113**, S68–S72 (2021).
3. Thapa, J., Gordon, S.V., Nakajima, C. & Suzuki, Y. Threat from Mycobacterium orygis-associated tuberculosis in South Asia. *Lancet Microbe* **3**, e641–e642 (2022).
4. Abdelsadek, H.A. et al. Multidrug-resistant strains of Mycobacterium complex species in Egyptian farm animals, veterinarians, and farm and abattoir workers. *Vet. World* **13**, 2150–2155 (2020).
5. Srinivasan, S. et al. Prevalence of Bovine Tuberculosis in India: a systematic review and meta-analysis. *Transbound. Emerg. Dis.* **65**, 1627–1640 (2018).
6. Ramanujam, H. & Palaniyandi, K. Bovine tuberculosis in India: the need for One Health approach and the way forward. *One Health* **16**, 100495 (2023).
7. McLoughlin, K.E. et al. RNA-Seq transcriptome analysis of peripheral blood from cattle infected with mycobacterium bovis across an experimental time course. *Front. Vet. Sci.* **8**, 662002 (2021).
8. Malone, K.M. et al. Comparative 'omics analyses differentiate Mycobacterium tuberculosis and Mycobacterium bovis and reveal distinct macrophage responses to infection with the human and bovine *tubercle bacilli*. *Micro. Genom.* **4**, e000163 (2018).
9. Killick, K.E. et al. Key hub and bottleneck genes differentiate the macrophage response to virulent and attenuated *Mycobacterium bovis*. *Front. Immunol.* **5**, 422 (2014).
10. Pu, W. et al. Comparative transcriptomic analysis of THP-1-derived macrophages infected with Mycobacterium tuberculosis H37Rv, H37Ra and BCG. *J. Cell Mol. Med.* **25**, 10504–10520 (2021).
11. Hasankhani, A. et al. In-depth systems biological evaluation of bovine alveolar macrophages suggests novel insights into molecular mechanisms underlying Mycobacterium bovis infection. *Front. Microbiol.* **13**, 1041314 (2022).
12. Abdelaal, H.F.M., Thacker, T.C., Wadie, B., Palmer, M.V. & Talaat, A.M. Transcriptional profiling of early and late phases of bovine tuberculosis. *Infect. Immun.* **90**, e0031321 (2022).
13. Nalpas, N.C. et al. Whole-transcriptome, high-throughput RNA sequence analysis of the bovine macrophage response to Mycobacterium bovis infection in vitro. *BMC Genom.* **14**, 230 (2013).
14. Ma, Y. et al. A species-specific activation of Toll-like receptor signaling in bovine and sheep bronchial epithelial cells triggered by Mycobacterial infections. *Mol. Immunol.* **71**, 23–33 (2016).
15. Remot, A. et al. Mycobacterial infection of precision-cut lung slices reveals type 1 interferon pathway is locally induced by Mycobacterium bovis but not M. tuberculosis in a Cattle Breed. *Front Vet. Sci.* **8**, 696525 (2021).
16. Braian, C., Svensson, M., Brighenti, S., Lerm, M. & Parasa, V. R. A 3D Human lung tissue model for functional studies on Mycobacterium tuberculosis Infection. *J. Vis. Exp*. https://doi.org/10.3791/53084 (2015).
17. Mukundan, S. et al. 3D host cell and pathogen-based bioassay development for testing anti-tuberculosis (TB) drug response and modeling immunodeficiency. *Biomol. Concepts* **12**, 117–128 (2021).
18. Surolia, R. et al. 3D pulmospheres serve as a personalized and predictive multicellular model for assessment of antifibrotic drugs. *JCI Insight* **2**, e91377 (2017).
19. Duval, K. et al. Modeling physiological events in 2D vs. 3D cell culture. *Physiology***32**, 266–277 (2017).
20. Baptista, D. et al. 3D Lung-on-chip model based on biomimetically microcurved culture membranes. *ACS Biomater. Sci. Eng.* **8**, 2684–2699 (2022).
21. Kang, D. et al. All-inkjet-printed 3D alveolar barrier model with physiologically relevant microarchitecture. *Adv. Sci.***8**, 2004990 (2021).
22. Jensen, C. & Teng, Y. Is it time to start transitioning from 2D to 3D cell culture. *Front. Mol. Biosci.* **7**, 33 (2020).
23. Whelan, A.O. et al. Revisiting host preference in the Mycobacterium tuberculosis complex: experimental infection shows M. tuberculosis H37Rv to be avirulent in cattle. *PLoS One* **5**, e8527 (2010).
24. Villarreal-Ramos, B. et al. Experimental infection of cattle with Mycobacterium tuberculosis isolates shows the attenuation of the human tubercle bacillus for cattle. *Sci. Rep.* **8**, 894 (2018).
25. McKee, C. & Chaudhry, G.R. Advances and challenges in stem cell culture. *Colloids Surf. B Biointerfaces* **159**, 62–77 (2017).
26. Dai, Y. et al. WebCSEA: web-based cell-type-specific enrichment analysis of genes. *Nucleic Acids Res.* **50**, W782–W790 (2022).
27. Shao, X. et al. MatrisomeDB 2.0: 2023 updates to the ECM-protein knowledge database. *Nucleic Acids Res.* **51**, D1519–D1530 (2023).
28. Kumar, R. et al. Divergent proinflammatory immune responses associated with the differential susceptibility of cattle breeds to tuberculosis. *Front. Immunol.* **14**, 1199092 (2023).
29. Gupta, V. K. et al. 3D Hydrogel Culture System Recapitulates Key Tuberculosis Phenotypes and Demonstrates Pyrazinamide Efficacy. *Adv. Healthc. Mater*. **14**, e2304299 (2024).
30. Magee, D.A. et al. Global gene expression and systems biology analysis of bovine monocyte-derived macrophages in response to in vitro challenge with Mycobacterium bovis. *PLoS One* **7**, e32034 (2012).
31. Chai, Q. et al. Lung gene expression signatures suggest pathogenic links and molecular markers for pulmonary tuberculosis, adenocarcinoma and sarcoidosis. *Commun. Biol.* **3**, 604 (2020).
32. Reichmann, M.T. et al. Integrated transcriptomic analysis of human tuberculosis granulomas and a biomimetic model identifies therapeutic targets. *J. Clin. Investig.* **131**, e148136 (2021).
33. Bhowmick, S. K. et al. Genomic signature of drug resistance and in vivo hypervirulence in *Mycobacterium Orygis*: decoding the blueprint of an emerging tuberculosis threat. *Available at SSRN 4735620*.
34. Almeida, P.E. et al. Mycobacterium bovis bacillus Calmette-Guerin infection induces TLR2-dependent peroxisome proliferator-activated receptor gamma expression and activation: functions in inflammation,

lipid metabolism, and pathogenesis. *J. Immunol.* **183**, 1337–1345 (2009).
35. Yu, D.S., Wu, C.L., Ping, S.Y., Keng, C. & Shen, K.H. Bacille Calmette-Guerin can induce cellular apoptosis of urothelial cancer directly through toll-like receptor 7 activation. *Kaohsiung J. Med. Sci.* **31**, 391–397 (2015).
36. Moreira-Teixeira, L. et al. Type I IFN exacerbates disease in tuberculosis-susceptible mice by inducing neutrophil-mediated lung inflammation and NETosis. *Nat. Commun.* **11**, 5566 (2020).
37. Moreira-Teixeira, L., Mayer-Barber, K., Sher, A. & O'Garra, A. Type I interferons in tuberculosis: foe and occasionally friend. *J. Exp. Med* **215**, 1273–1285 (2018).
38. Dey, R.J. et al. Inhibition of innate immune cytosolic surveillance by an M. tuberculosis phosphodiesterase. *Nat. Chem. Biol.* **13**, 210–217 (2017).
39. Dey, B. et al. A bacterial cyclic dinucleotide activates the cytosolic surveillance pathway and mediates innate resistance to tuberculosis. *Nat. Med.* **21**, 401–406 (2015).
40. Gong, W.P. et al. Effects of Mycobacterium vaccae vaccine in a mouse model of tuberculosis: protective action and differentially expressed genes. *Mil. Med. Res.* **7**, 25 (2020).
41. Covian, C. et al. BCG-induced cross-protection and development of trained immunity: implication for vaccine design. *Front. Immunol.* **10**, 2806 (2019).
42. Lin, P.L., Plessner, H.L., Voitenok, N.N. & Flynn, J.L. Tumor necrosis factor and tuberculosis. *J. Investig. Dermatol. Symp. Proc.* **12**, 22–25 (2007).
43. Allie, N. et al. Prominent role for T cell-derived tumour necrosis factor for sustained control of Mycobacterium tuberculosis infection. *Sci. Rep.* **3**, 1809 (2013).
44. Yamamoto, T. et al. Mycobacterium bovis BCG vaccination modulates TNF-alpha production after pulmonary challenge with virulent Mycobacterium tuberculosis in guinea pigs. *Tuberculosis***87**, 155–165 (2007).
45. Ehlers, S. Role of tumour necrosis factor (TNF) in host defence against tuberculosis: implications for immunotherapies targeting TNF. *Ann. Rheum. Dis.* **62**, ii37–ii42 (2003).
46. Lui, G. et al. HMGB1/RAGE signaling and pro-inflammatory cytokine responses in non-HIV adults with active pulmonary tuberculosis. *PLoS One* **11**, e0159132 (2016).
47. da Silva, L.F. et al. Advanced glycation end products (AGE) and receptor for AGE (RAGE) in patients with active tuberculosis, and their relationship between food intake and nutritional status. *PLoS One* **14**, e0213991 (2019).
48. Lin, L., Park, S. & Lakatta, E.G. RAGE signaling in inflammation and arterial aging. *Front Biosci. (Landmark Ed.)* **14**, 1403–1413 (2009).
49. Machahua, C. et al. Increased AGE-RAGE ratio in idiopathic pulmonary fibrosis. *Respir. Res.* **17**, 144 (2016).
50. Almeida, P.E., Carneiro, A.B. & Silva, A.R. & Bozza, P. T. PPARgamma expression and function in mycobacterial infection: roles in lipid metabolism, immunity, and bacterial killing. *PPAR Res* **2012**, 383829 (2012).
51. Arnett, E. et al. PPARgamma is critical for Mycobacterium tuberculosis induction of Mcl-1 and limitation of human macrophage apoptosis. *PLoS Pathog.* **14**, e1007100 (2018).
52. Wu, L. et al. IRF1 as a potential biomarker in Mycobacterium tuberculosis infection. *J. Cell Mol. Med.* **25**, 7270–7279 (2021).
53. Delemarre, E.M. et al. Serum biomarker profile including CCL1, CXCL10, VEGF, and adenosine deaminase activity distinguishes active from remotely acquired latent tuberculosis. *Front Immunol.* **12**, 725447 (2021).
54. Zhao, Y. et al. IP-10 and RANTES as biomarkers for pulmonary tuberculosis diagnosis and monitoring. *Tuberculosis***111**, 45–53 (2018).
55. Selvavinayagam, S. T. et al. Plasma CXCL8 and MCP-1 as surrogate plasma biomarkers of latent tuberculosis infection among household contacts-A cross-sectional study. *PLOS Glob. Public Health* **3**, e0002327 (2023).
56. Robson, S.C. et al. Acute-phase response and the hypercoagulable state in pulmonary tuberculosis. *Br. J. Haematol.* **93**, 943–949 (1996).
57. Turken, O. et al. Hemostatic changes in active pulmonary tuberculosis. *Int. J. Tuberc. Lung Dis.* **6**, 927–932 (2002).
58. Lee, M.J. et al. Identification of human complement factor B as a novel biomarker candidate for pancreatic ductal adenocarcinoma. *J. Proteome Res.* **13**, 4878–4888 (2014).
59. Coad, M. et al. Simultaneous measurement of antigen-induced CXCL10 and IFN-gamma enhances test sensitivity for bovine TB detection in cattle. *Vet. Microbiol.* **230**, 1–6 (2019).
60. Nalpas, N.C. et al. RNA sequencing provides exquisite insight into the manipulation of the alveolar macrophage by tubercle bacilli. *Sci. Rep.* **5**, (2015). 13629.
61. Ravi, M., Paramesh, V., Kaviya, S.R., Anuradha, E. & Solomon, F.D. 3D cell culture systems: advantages and applications. *J. Cell Physiol.* **230**, 16–26 (2015).
62. Jain, R. et al. Enhanced and enduring protection against tuberculosis by recombinant BCG-Ag85C and its association with modulation of cytokine profile in lung. *PLoS One* **3**, e3869 (2008).
63. Zhang, F. & Kang, H.M. FASTQuick: rapid and comprehensive quality assessment of raw sequence reads. *Gigascience* **10**, (2021).
64. Chen, S., Zhou, Y., Chen, Y. & Gu, J. fastp: an ultra-fast all-in-one FASTQ preprocessor. *Bioinformatics* **34**, i884–i890 (2018).
65. Ewels, P., Magnusson, M., Lundin, S. & Kaller, M. MultiQC: summarize analysis results for multiple tools and samples in a single report. *Bioinformatics* **32**, 3047–3048 (2016).
66. Dobin, A. et al. STAR: ultrafast universal RNA-seq aligner. *Bioinformatics* **29**, 15–21 (2013).
67. Liao, Y., Smyth, G.K. & Shi, W. featureCounts: an efficient general purpose program for assigning sequence reads to genomic features. *Bioinformatics* **30**, 923–930 (2014).
68. Love, M.I., Huber, W. & Anders, S. Moderated estimation of fold change and dispersion for RNA-seq data with DESeq2. *Genome Biol.* **15**, 550 (2014).
69. Blighe, K., et al. Enhanced Volcano: publication-ready volcano plots with enhanced colouring and labeling, https://github.com/kevinblighe/EnhancedVolcano. (2018).
70. Reimand, J. et al. Pathway enrichment analysis and visualization of omics data using g: Profiler, GSEA, Cytoscape and EnrichmentMap. *Nat. Protoc.* **14**, 482–517 (2019).
71. Chin, C., Chen, S. H., Wu, H. H. cytoHubba: identifying hub objects and sub-networks from complex interactome. *BMC Syst. Biol*. https://doi.org/10.1186/1752-0509-8-S4-S11 (2014).
72. Zhao, T. & Wang, Z. GraphBio: a shiny web app to easily perform popular visualization analysis for omics data. *Front. Genet.* **13**, 957317 (2022).

Acknowledgements

Financial support as an intramural grant from the National Institute of Animal Biotechnology, and an extramural grant (No. BT/PR31378/AAQ/1/745/2019) from the Department of Biotechnology (DBT), Govt. of India are thankfully acknowledged. Support by DBT for providing Junior Research Fellowship (JRF) to V.B., and JRF/SRF to R.K.; Council for Scientific and Industrial Research for JRF/SRF to M.R.P.; Department of Science and Technology (DST), Govt. of India for providing the Inspire fellowship (JRF) to S.G. are thankfully acknowledged. We are thankful to Dilna S V, Nilanjana Ganguli, and Shashikant Gawai for technical help with the LC-MS analysis, and Microscopic Imaging. We acknowledge Prof. Sharmistha Banerjee, Co-ordinator of the UoH-NIAB BSL3 facility, University of Hyderabad, India, and other technical staff for supporting the BSL3-based experiments.

Author contributions

Conceived the project: B.D. Conceived and designed the experiments: V.B., B.D. Performed the experiments: V.B., R.K., S.G., H.K.M., U.S., B.D. Analyzed the data: V.B., R.K., M.R.P., U.S., B.D. Contributed reagents/materials/analysis tools/facility: B.D., U.S. Wrote the paper: V.B., R.K., B.D. provided overall supervision throughout the study: B.D.

Competing interests

The authors declare no competing interests.

Additional information

Supplementary information The online version contains supplementary material available at https://doi.org/10.1038/s42003-025-07883-6.

Correspondence and requests for materials should be addressed to Bappaditya Dey.

Peer review information *Communications Biology* thanks Paul Cos, Ranu Surolia, and Vivek Kapur for their contribution to the peer review of this work. Primary Handling Editors: Ngan Huang and Tobias Goris. A peer review file is available.